

A Guide to the Solidification of Steels



Jernkontoret, Stockholm 1977.

Jernkontoret
Box 1721
S-111 87 Stockholm

Ljungberg Tryckeri AB, Södertälje 1977

ISBN 91-7260-156-6

FOREWORD

An investigation into the solidification structures in steels of commercial interest was started by Jernkontoret in 1974. The planning and supervision of work was the responsibility of a Research Committee, having the Jernkontoret reference of 408/74. Membership of this Committee comprised:

G. Grünbaum, (Sandvik AB), Chairman, B. Callmer, (Swedish Institute for Metals Research), Secretary, Ö. Hammar, (Sandvik AB), P. Havola, (Ovako Oy), L. Hellner, (AB Bofors), S. Malm, (Uddeholms AB), L. Morsing, (Avesta Jernverks AB) and Å. Nilsson, (Stora Kopparberg AB).

The experimental programme was carried out at the Swedish Institute for Metals Research, Stockholm, where initially B. Carlsson and, from 1975, B. Callmer, were responsible for the work, including evaluation of results. Metallography and photomicrography were performed by H. Modin. The companies represented on the Committee supplied samples of steels and made other contributions to the experimental programme. D. Dulieu (BSC, Sheffield Laboratories, England), assisted with the preparation of the English text. The project was partly financed by the Swedish Board for Technical Development.



CONTENTS

Foreword	5
Introduction	9
1. Experimental Techniques	11
2. Carbon and Low Alloy Steels	17
3. Chromium Steels	55
4. Stainless and Heat Resistant Steels	81
5. High Speed Steels	133
6. Conclusions and Comments	142
7. References	151
8. Alloy Index	154



INTRODUCTION

The purpose of the present work is to provide a systematic compilation of solidification data, describing the formation of the as-cast microstructures in steels of technical importance. The compositions have been chosen to cover a large part of the spectrum of steels in current production. Where a specific steel is not included, it should be possible to gain an outline of its solidification characteristics from related compositions present.

The book is not intended to provide a theoretical treatment of solidification processes in steels. It is hoped rather that the descriptions of the microstructures formed on solidification will assist in solving, or avoiding, some of the problems arising in casting, hot working and welding. However, specific production and materials problems have not been described. A knowledge of solidification processes is also relevant to problems of quality in the final product; for example, in understanding the effects of segregation arising during solidification on the microstructure of wrought material. The work should find use also in metallurgical education as a source of basic information.

In the planning stage, the Project Committee hoped to collect data from both the technical literature and unpublished laboratory reports. However, a study of these sources soon showed that most investigations were unique in both their experimental techniques and presentation of results. In addition, thermal analysis at varying cooling rates had been identified in this project as a powerful technique for investigation of solidification. Little systematic experimental work employing this method was found in the literature. It was decided, therefore, to generate the data needed within the study and to use the same reproducible methods for all the steel compositions studied.

The Committee gave considerable attention to the problem of relating structures obtained in small, laboratory ingots to those found in large ingots under production conditions. This aspect is discussed in chapter 1, where the experimental techniques are described and the format adopted for diagrams and tables is explained.

Chapters 2–5 comprise the main body of the book, with results for each individual steel described. These sections are printed in a standardized form for ease of quick reference. The large number of steels has made it necessary to limit the amount of information given. Wherever possible in these chapters, descriptive passages have been avoided in favour of figures, diagrams and micrographs.

The alloys have been brought together into four broad classes:

Carbon and Low Alloy Steels	(Ch. 2)
Chromium Steels	(Ch. 3)
Stainless and Heat Resistant Steels	(Ch. 4)
High Speed Steels	(Ch. 5)

Although the intention was to arrange the steels in a logical way, this was not always possible. In most cases, however, a steel type will be classified easily within the four groups.

Each of chapters 2 to 5 is introduced by a paragraph describing those specific steels which have been studied. The reader can quickly ascertain whether a steel composition is included or not, by examining either the tables accompanying each chapter, or the index tables given in chapter 8.

Chapter 6 contains some general conclusions regarding solidification phenomena which are common for the groups of steels. References to the relevant literature have been made throughout and are listed in full in chapter 7.

Chapter 8 comprises master tables of chemical compositions and thermal analysis data for all the steels included in the study. In addition, this chapter includes tables of dendrite arm spacings and microsegregation.



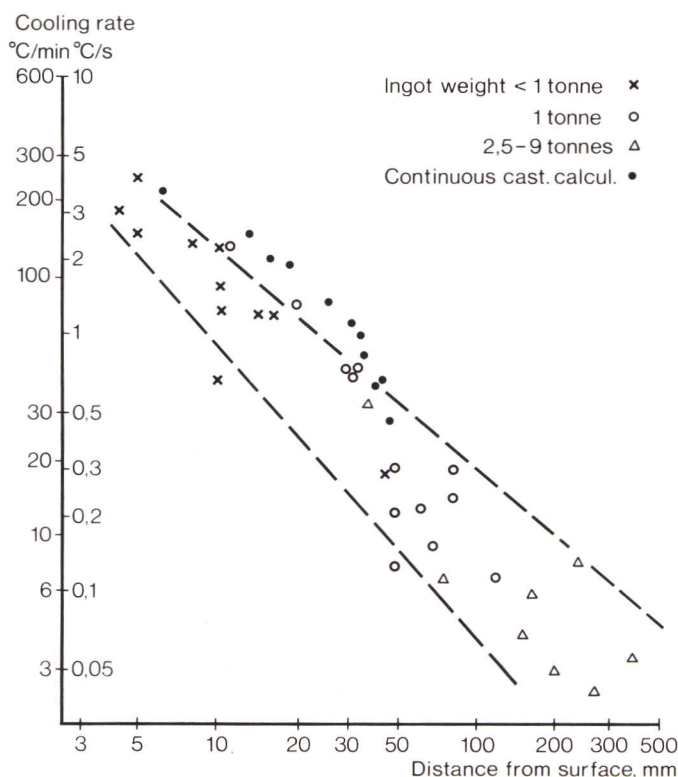
1. Experimental Techniques

The object of the laboratory experiments was to produce microstructures identical to those obtained under production solidification conditions. A suitable experimental technique would allow the following:

- Determination of pertinent temperatures, such as those of the liquidus, solidus and high temperature reactions, together with the relative amounts of the phases formed.
- The ability to freeze instantaneously the solidification reaction by rapid quenching.
- A controlled cooling rate which could be varied within wide limits.
- A reproducible relationship between the structures obtained in laboratory samples and those found in full-size ingots.

To fulfill these requirements, the experiments were carried out on small ingots (35 g) solidified in a ceramic crucible at a preset, controlled cooling rate. The development of the solidification microstructure is governed mainly by alloy composition and the rate of heat removal. By using samples of commercial alloys and letting them cool at a rate similar to that found in full scale ingots, good reproduction of microstructural features was obtained.

A range of cooling rates in steel ingots, evaluated from published cooling curves, is shown in figure 1.1, [1–4, 23, 26, 93, 96]*. The results refer to different ingot sizes; which means that values on the abscissa are only indicative of position within an ingot. The figure shows that the range of cooling rates of practical interest lies between 0,05 and 3°C/s. Accordingly, the specimens in this study were cooled at 0,1, 0,5 and 2°C/s.



* References appear in chapter 7

Figure 1.1 Cooling rates in steel ingots and continuously cast billets

According to reported data (for cooling rates [20], solidification rates [4, 21] and local solidification times [22]), ingots produced by the electroslag remelting or vacuum arc remelting processes follow, in general, the pattern shown in figure 1.1.

No experimental values of cooling rates in continuous casting were found in the literature. Calculations based on mathematical models of heat transfer show these cooling rates to be slightly higher than for ingots up to 20–30 mm under the surface, as shown in figure 1.1 [5, 6]. At larger depths no great difference exists, as cooling rate is governed by heat conduction in the solidified shell. This has been established by comparisons between measured solidification speeds in ingots and continuously cast material, [4, 7, 8].

Solidification of weld metal takes place at high cooling rates. Depending on process parameters, such as the size of the weld pool, rates have been reported to vary between 20 and 200°C/s, [10, 11].

In powder metallurgy very high cooling rates are encountered. Calculations lead to an estimate of 10^3 – 10^4 °C/s for the solidification of argon atomized steel particles [9]. Welding and powder metallurgy are thus not directly covered by the experiments reported in the present work.

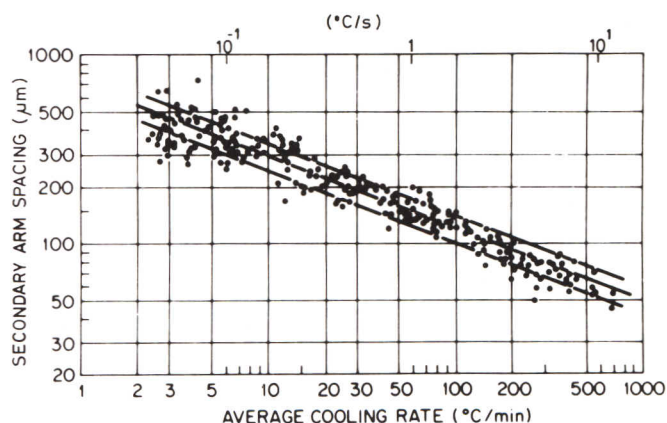


Figure 1.2 Dendrite arm spacings in commercial 0,14–0,88% C-steel ingots (After Suzuki A. et al, *J. Japan Inst. of Metals*, (1968) 1301–1305.) [28]

The cooling rate may be related to the microstructure through its effect on the secondary dendrite arm spacing. This decreases with increasing cooling rate in the manner shown in figure 1.2, [28]. Many diagrams of this type are available in the literature. When extrapolated to cooling rates prevailing in welding and powder solidification, the relationship predicts fairly well the secondary dendrite arm spacings in weld metal and steel powder, [14, 9, 96]. As shown in later sections, the arm spacings found in the small samples are of the same order of magnitude as those reported for ingots of the same composition. Figure 1.3 shows examples of secondary dendrite arm spacing measurements in the columnar zones of ingots of low alloy steel ranging in weight from 1 to 9 tonnes, together with results from a 1,7 tonne stainless ingot, [12, 13, 26].

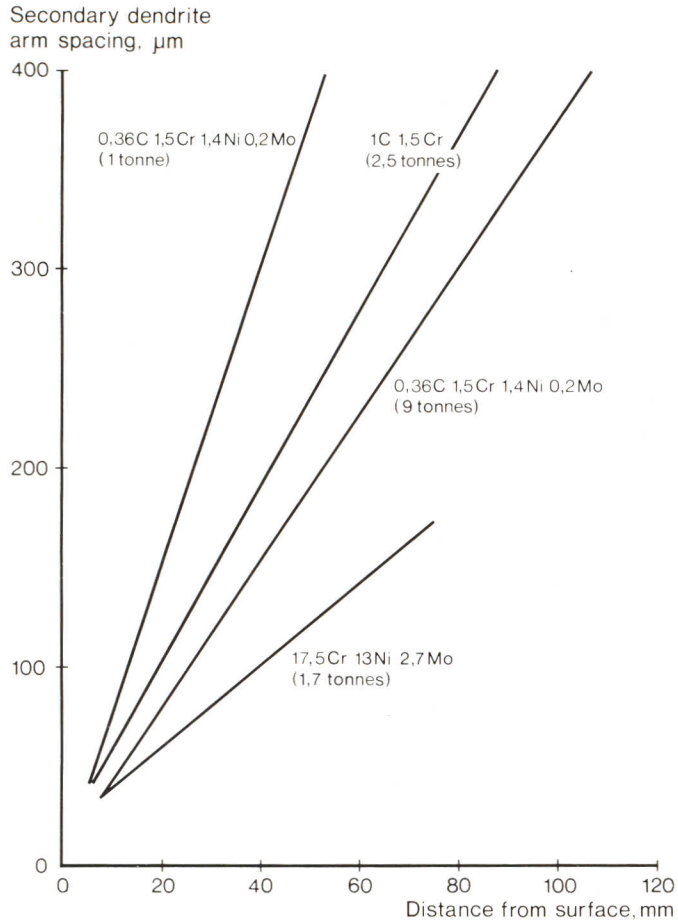


Figure 1.3 Dendrite arm spacings in production scale ingots

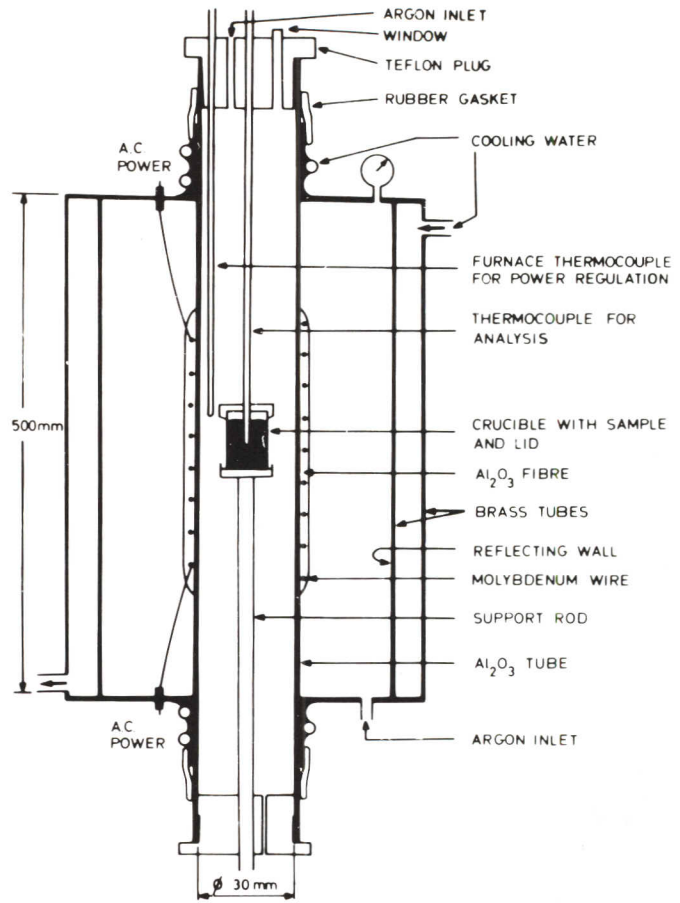


Figure 1.4 Experimental furnace

Thermal analysis

The steel samples of 35 ± 1 g were melted in alumina crucibles in an atmosphere of argon ($O_2 < 5$ ppm). Samples inserted in the hot furnace, shown in figure 1.4, melted in five minutes.

A tube of alumina was resistance heated by a molybdenum wire element. Argon was flushed through the tube from the top at a rate of approximately 0,1 l/s. The outside of the tube with the molybdenum wire was subjected to a non-flowing argon atmosphere. The tubular furnace shell was double-walled and water cooled, with the inside chromium plated to give good heat reflection. No insulation was used so that the furnace had a low thermal inertia, enabling cooling rates of up to 2.0°C/s to be achieved down to 1000°C . The samples were quenched in brine within about three seconds from removal at the bottom of the furnace.

The temperature and cooling rate of the furnace was controlled by the power input. The desired furnace cooling rate was achieved by presetting a programmable temperature-time regulator (Data Trak). An artificial thermoelectric voltage-time function was generated and compared with the actual output of the furnace thermocouple. The system minimized any difference by adjusting the furnace power input. The accuracy in cooling rate which was obtained was better than ten percent. Figure 1.5 shows schematically the regulating and measuring system of the furnace.

The temperature of the steel sample was measured at its centre by means of a thermocouple (Pt/Pt-10% Rh). The thermocouple output was registered by a digital microvolt meter. The cold junction was maintained at 0°C . One registration of specimen temperature per degree fall in furna-

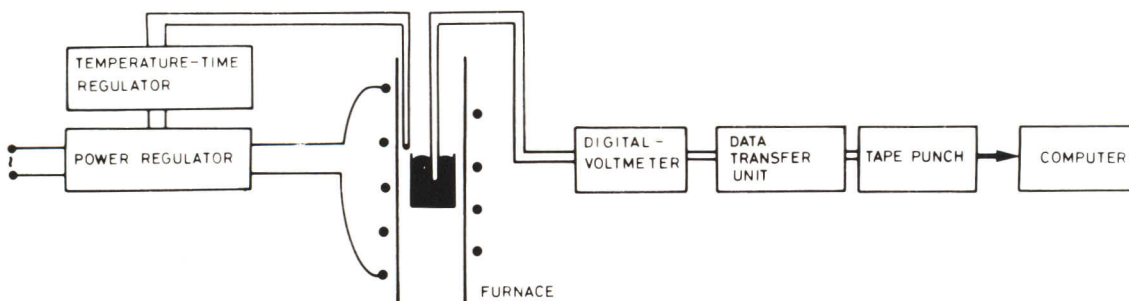


Figure 1.5 Control systems

ce temperature was used for all the cooling rates. The result was punched on a paper tape and evaluated in a minicomputer. The thermocouples and the other components used were checked by determining the liquidus temperature of a pure nickel melt. The precision of the temperature measurements was found to be $\pm 2^\circ\text{C}$.

Thermal analysis, as used here, is based on an analysis of the temperature versus time curve of a solidifying sample. The furnace and the molten sample are subject to a constant cooling rate, but when the sample starts to solidify the latent heat evolved decreases the cooling rate of the sample. In fact, all reactions or transformations evolving latent heat decrease the cooling rate of the sample. The growth of the solid phase starts at the walls of the crucible and proceeds to the centre. The dendrites grow at an almost constant temperature, shown by the plateau of the temperature-time curve in figure 1.6. When the tips of the dendrites reach the thermocouple the heat transfer from the thermocouple becomes markedly more rapid and the amount of latent heat sensed by the thermocouple is diminished. As a consequence the registered temperature starts to decrease.

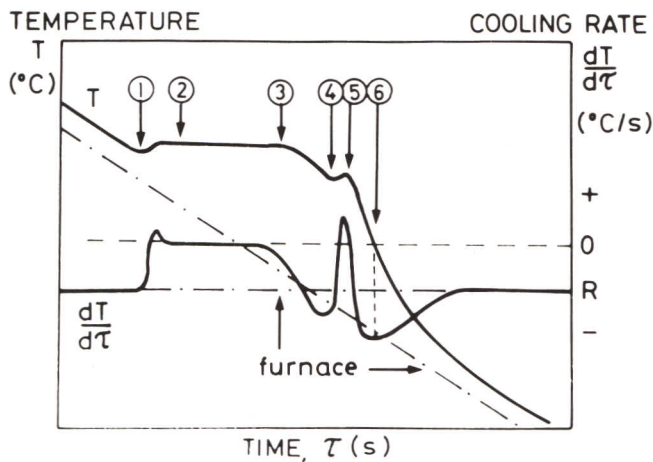


Figure 1.6 Thermal analysis, temperatures and events:

- ① Start of growth of primary phase
- ② Growth temperature of dendrites, used as liquidus temperature
- ③ Dendrite tips reach thermocouple in centre of sample
- ④ Start of secondary phase precipitation
- ⑤ Maximum reaction rate for secondary phase precipitation, maximum temperature, used as temperature of formation of the secondary phase
- ⑥ End of solidification, used as solidus temperature
- R Preset cooling rate of furnace

The temperature of the plateau was taken as the liquidus temperature in this work. This temperature is slightly lower than that of the true equilibrium liquidus, but the difference is very small and of no practical significance. Supercooling was generally observed before nucleation and growth. The degree of supercooling was generally larger and more varied at the start of the secondary (peritectic) reaction than for primary (ferrite) nucleation in the solidification of a ferritic-austenitic steel. The temperatures given for the secondary phase formation are thus less accurate than those of the primary phase formation (liquidus). The end of solidification was defined as the temperature at which the temperature-time curve had its inflection point, that is, where the cooling rate $\frac{dT(\tau)}{d\tau}$ reached

a minimum, see figure 1.6. After this point the cooling rate of the sample started to approach the cooling rate of the furnace, since no more latent heat was evolved. The derivative is more useful for evaluation of the cooling curve, showing changes more clearly than the temperature-time curve itself.

The end of solidification, as defined here, is denoted the solidus temperature and is strongly dependent on the cooling rate. It was particularly difficult to determine the solidus temperature by thermal analysis in steels with a high carbon content. This is a result of their wide solidification ranges and very low growth rates near the end of solidification. Furthermore, eutectic reactions occurred at the end of solidification over a large temperature range which led to poorly defined minima in the derivative.

The solidus temperature was also determined as the start of melting in heating tests. The samples cooled at 0,1 and 0,5°C/s were reheated at 0,5°C/s. The start of melting and the end of solidification in cooling trials generally differed only by a few degrees. The lowest of these temperatures was chosen as the solidus temperature and rounded off to within five degrees. Quenching experiments confirmed that this method for determining the solidus temperature was acceptable. In a few cases a small amount of the melt could solidify below the reported solidus temperature, but for practical purposes the reported solidus temperatures are relevant.

All temperatures given in the tables are mean values of two to five measurements and thus are not necessarily those which can be evaluated from the cooling curves shown.

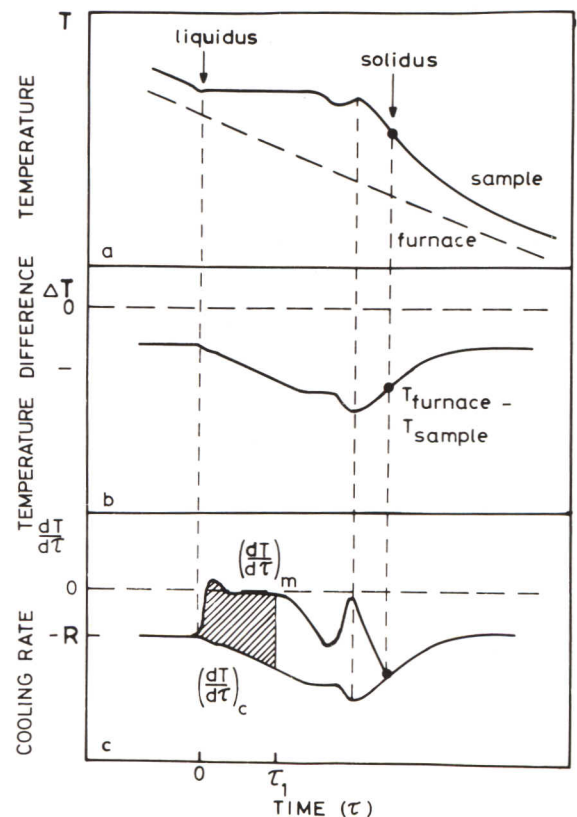


Figure 1.7 a-c. Derivation of fraction solid phase.

The fraction solid phase, f_s , as a function of time was calculated using the following principles [90]. When the sample starts to solidify, latent heat, L , is evolved which decreases the cooling rate $\frac{dT}{d\tau}$ as shown in figure 1.7 a and c. The cooling rate of the furnace is not affected and thus the temperature difference, ΔT , between the furnace and the sample is increased, and varies according to the curve in figure 1.7 b. The temperature difference is related to the heat flux $\frac{dQ}{d\tau}$ from the sample to the furnace, and $\frac{dQ}{d\tau}$, will vary in the same way as ΔT .

Assuming $\delta Q = C_p \cdot \delta T$, (where C_p is the specific heat), a calculated cooling rate, $\left(\frac{dT}{d\tau}\right)_c$, corresponding to the heat flux $\frac{dQ}{d\tau}$ can be derived as follows, see figure 1.7 c.

$$\left(\frac{dT}{d\tau}\right)_c = \frac{1}{C_p} \cdot \frac{dQ}{d\tau}$$

The difference between the measured cooling rate $\left(\frac{dT}{d\tau}\right)_m$ and $\left(\frac{dT}{d\tau}\right)_c$ is the evolution of latent heat in the sample.

$$\frac{dL}{d\tau} = C_p \cdot \left[\left(\frac{dT}{d\tau}\right)_m - \left(\frac{dT}{d\tau}\right)_c \right]$$

Hence the area between the two curves in figure 1.7 c is proportional to L_{τ_1} , the latent heat evolved in the interval 0 to τ_1 .

$$L_{\tau_1} = \int_0^{\tau_1} \frac{dL}{d\tau} d\tau = \int_0^{\tau_1} C_p \left[\left(\frac{dT}{d\tau}\right)_m - \left(\frac{dT}{d\tau}\right)_c \right] d\tau$$

The latent heat evolved is proportional to the fraction solid phase at the time considered. As $\frac{dQ}{d\tau}$ is not readily measured, an approximation of $\left(\frac{dT}{d\tau}\right)_c$ was obtained using the cooling rates measured at the start and end of solidification. In an iterative process, the calculated fraction solid phase was used to improve the approximate value of $\left(\frac{dT}{d\tau}\right)_c$.

This analysis is the basis for computing the fraction solid phase. The calculations were more elaborate than the simplified analysis indicates. Corrections, such as for the different specific heats of the liquid and solid phases and their relative amounts during solidification, were included in the actual computation.

The results of these calculations are given graphically on the upper part of each solidification diagram and in the tables of thermal analysis data.

Alternative methods of calculating fraction solid phase are given in references [16–19].

Metallographic Examination

Metallographic examination of samples was carried out after mechanical preparation and etching in a range of solutions appropriate to the individual steel composition, [15].

The dendritic structure was revealed by the following etching techniques:

Steel Type	Etchant
Carbon, low alloy and 5% chromium steels.	Saturated solution of picric acid in water or a mixture of water and alcohol.
13% chromium, stainless and heat resistant steels.	Various etchants according to the etching behaviour of the respective alloy. a) Copper-containing reagents (Steads). b) Mixed acids, HNO ₃ , HCl and water in proportion by volume 1:10:10 with the addition of some drops of pickling bath inhibitor.* (Used at 65°C) c) Acid ferric chloride, FeCl ₃ , HCl and water in various proportions. (Used cold or warm)
High speed steels	Normally 4% nital solution. For examination at higher magnification alkaline permanganate was used (4 wt% NaOH saturated with KMnO ₄).

Table 1.1 Summary of etchants

* In general, this etching reagent gives only a gentle surface relief and no selective darkening. To reveal the dendrites clearly the following technique has been used: The structure is under- or overfocussed, depending on where the best image is obtained, and simultaneously the aperture diaphragm is stopped down considerably in order to increase the depth of focus. In this way a sharp image with good contrast is obtained, i.e. light with dark boundaries or vice versa depending on whether it is under- or overfocussed.

Where both γ - and δ -dendrites are formed the γ -dendrites appear white and the area occupied by the δ -dendrites dark at low magnification (figure 1.8 a). The reason for this is that, on cooling and quenching, the δ -dendrites are partly transformed to γ which contains closely spaced networks of residual δ , figure 1.8 b.

To reveal dendritic and interdendritic ferrite, carbides, phosphides and intermetallic phases, appropriate etchants for the steels in question were used [15]. In some cases the visual observations were supported by identification of the phases using microprobe analysis, X-ray diffraction and transmission electron microscopy.

The magnifications of the optical photomicrographs have been standardized as far as possible to facilitate comparisons between structures. (Micrographs have been reproduced at actual size, so that magnifications refer directly to the size ratio between objects in the sample and in the illustration).

Figure 1.8 a Stainless steel shown at low magnification, (steel number 407)

× 150 100 μm

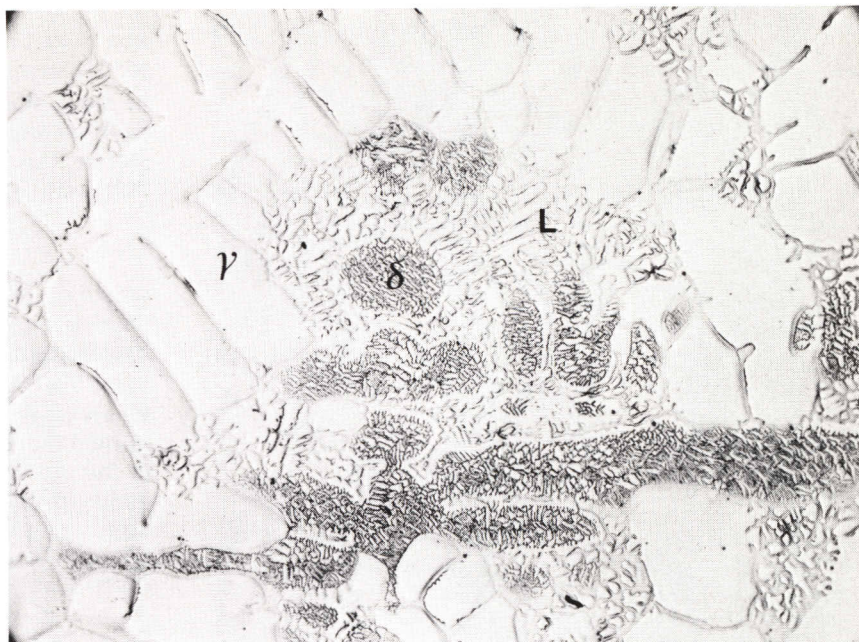
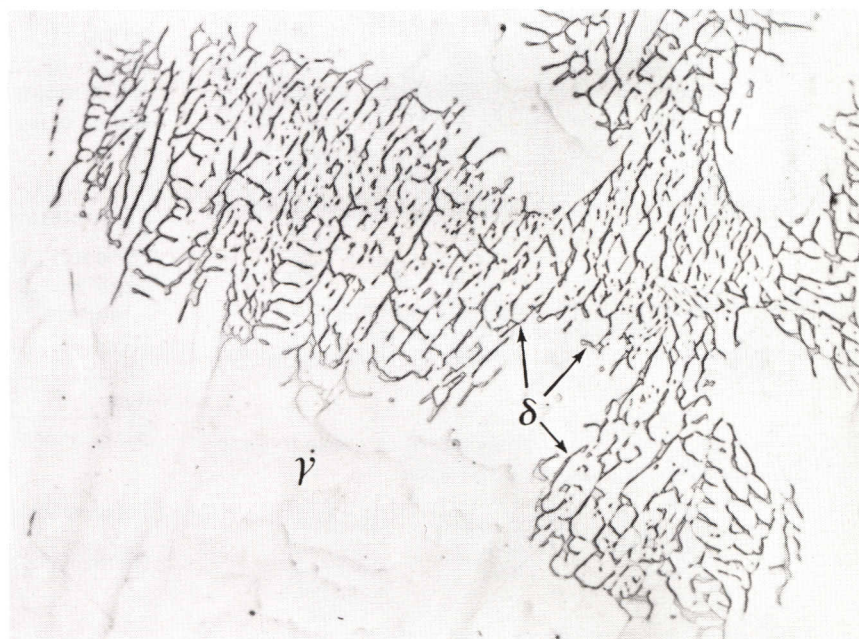


Figure 1.8 b Detail of figure 1.8 a showing transformed δ -areas

× 600 25 μm



The secondary dendrite arm spacings have been measured at a low magnification. The measurements were made close to and parallel with the parent primary dendrite stems (figure 1.9). At least four or five secondary arms per primary arm were counted and at least ten such measurements were taken within each steel specimen, where this was possible. The result reported is the arithmetic mean of the individual secondary arm spacings. In most samples a large number of observations was possible and the mean values have good statistical significance. Exceptions are the specimens obtained at the lowest cooling rate, because the large arm spacings in these samples limited the number of observations, together with the ferritic-austenitic stainless steels, in which a very low degree of segregation gave a correspondingly diffuse microstructure.

Structures arising from the quench itself, such as fine

transformation products, are in general not discussed in the figure captions.

Microsegregation

Microsegregation was studied by electron microprobe analysis of samples cooled at $0,5^\circ\text{C/s}$ and quenched from just below the solidus temperature. Line scans were performed in selected areas of the specimens. Before analysis the samples were etched and the lines to be traversed were marked with microhardness indentations. Strongly etched specimens were repolished before measuring. Two lines were selected from different areas in each specimen, on the same principle as that for selecting lines for dendrite arm measurement. Consequently, in most cases secondary dendrite arms were crossed at right angles but some primary dendrites were intersected also. A typical example of a traverse for analysis is shown in figure 1.9.

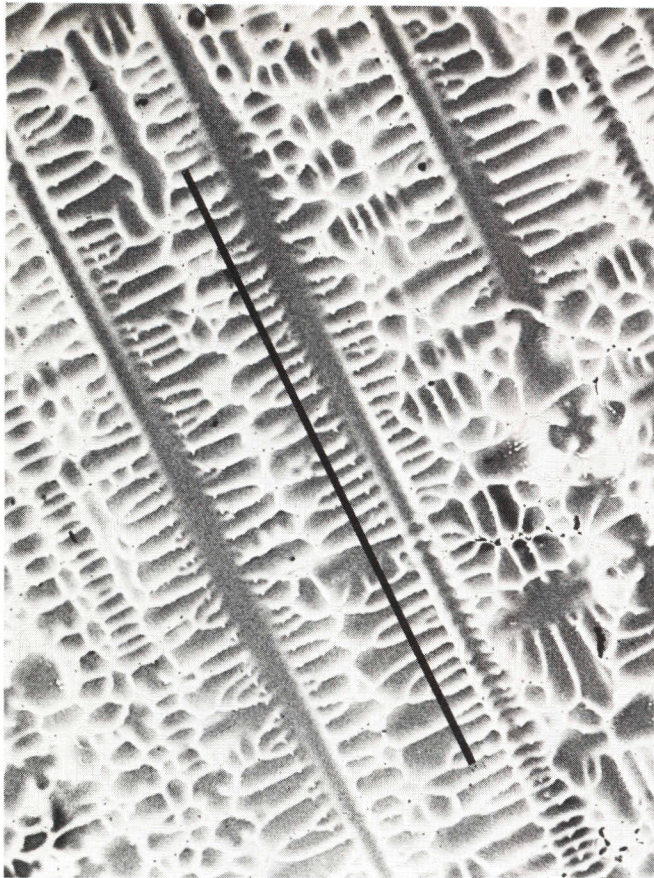


Figure 1.9 Primary and secondary dendrite arms in a typical field showing a traverse followed for the measurement of secondary dendrite arm spacings and electron microprobe analysis, (steel number 410).

The total lengths over which analyses were made in each steel and the scanning speeds used were:

	Carbon and low alloy steels	5% and 13% chromium steels	Stainless, heat resistant and high speed steels*
Distance	6000 μm	3000 μm	2800 μm
Speed	1,1 μm/s	0,7 μm/s	1,3 μm/s

* Microsegregation in high speed steels was also measured by point analysis.

For quantitative calibration, the X-ray intensities were compared with those of homogeneous standard specimens having accurately analyzed compositions close to those of the experimental samples.

From the microprobe analyses, mean solute concentration values were evaluated in dendritic and interdendritic areas. The segregation ratio (I) of the alloying element (x) from the centre of the dendrites (D) to the interdendritic areas (ID) was calculated as:

$$I = \frac{C_{x, ID}}{C_{x, D}}$$

where C_x is the mean concentration value. I has been calculated in a straightforward way when the segregation occurred within one phase such as ferrite or austenite. In two-phase steels there is, in addition to this segregation, partitioning of alloying elements between the phases, principally between austenite and ferrite. Partition ratios

are defined below and the appropriate values of segregation ratio, I , or partition ratios, P_{ID} or P_D , have been reported for each steel.

In many stainless steels, ferrite is precipitated from the residual melt in the interdendritic areas together with austenite, (for example in steel 407, figure 10), and a partition ratio P_{ID} has been calculated as:

$$P_{ID} = \frac{C_x, \delta_{ID}}{C_x, \gamma_{ID}}$$

where C_x is the mean value of the concentration of element x in interdendritic δ and γ . P_{ID} is thus a quantity describing the partition of the element x between interdendritic ferrite and austenite.

When austenite grew into and consumed dendrites which formed initially as ferrite, thin regions of ferrite remained in the austenite matrix in some stainless steels, (for example in steel 403, figure 7). This solid phase transformation also gives rise to partitioning of alloying elements between austenite and dendritic ferrite, and a partition ratio P_D may be calculated:

$$P_D = \frac{C_x, \delta_D}{C_x, \gamma_D}$$

where C_x is the mean value of the concentration of element x in δ and γ in dendritic areas. The specific problem of segregation and partition ratios in two-phase stainless steels is discussed further in chapter 6.

Presentation of results

For each type of steel the results are reported on one data page and at least one page with micrographs. The more important contents of these pages are explained in table 1.2:

Item	Definition
Designations	The corresponding Swedish, American and German standard steel designations
Composition	The chemical composition of the actual sample
Thermal analysis	The diagram on a data page represents a furnace cooling rate of $R=0,5^\circ\text{C/s}$; f_s indicates fraction solidified phase. The table contains mean values of pertinent temperatures obtained from two to five measurements at three cooling rates. The figures in circles refer to the arrows in the diagram. These relate to specific curves and may differ from mean values, they should be used as an aid to interpretation only. Solidification range defined as liquidus – solidus temperature, $^\circ\text{C}$ Solidification time defined as the time corresponding to the solidification range, s
Precipitates	Sulphides, carbides, nitrides and intermetallic phases found in the solidification structure.
Microsegregation	The results refer to samples cooled at $0,5^\circ\text{C/s}$ and quenched from $50-60^\circ\text{C}$ below the reported solidus temperature.
I, P_{ID}, P_D	Segregation and partition ratios as defined in detail above.
T_q	Quenching temperature, $^\circ\text{C}$
d	Secondary dendrite arm spacing, μm
δ and γ	Ferrite and austenite
L	Quenched liquid

Table 1.2 Key to presentation of experimental results

2. Carbon and Low Alloy Steels

The steels of this group represent the most common commercial steels. They are produced as ingots and castings of all sizes. Continuous casting is also widely used for all except the steels of the highest carbon content.

Carbon steels exist with carbon levels from below 0,1% to above 1,3%, depending upon the required strength and hardness. The carbon steels chosen are listed in table 2.1:

No.	C	Si	Mn	Others %
201	0,11	0,12	1,3	
202	0,12	0,3	1,5	
203	0,18	0,4	1,2	0,03 Nb
204	0,19	0,4	1,5	
205	0,36	0,3	0,6	
206	0,69	0,2	0,8	
207	1,01	0,3	0,5	

Table 2.1 Carbon steels

Steel 202 was treated with rare earth metals to modify the sulphide inclusions. The manganese and silicon concentrations are typical for silicon killed steels.

The carbon contents have been selected to represent the main solidification paths expected from the equilibrium diagram of the Fe-C system shown in figure 2.1. The solidification of steels with lower and higher carbon contents can be extrapolated.

The types of solidification are:

- primary ferrite formation
- primary ferrite formation followed by a peritectic reaction
- primary austenite formation

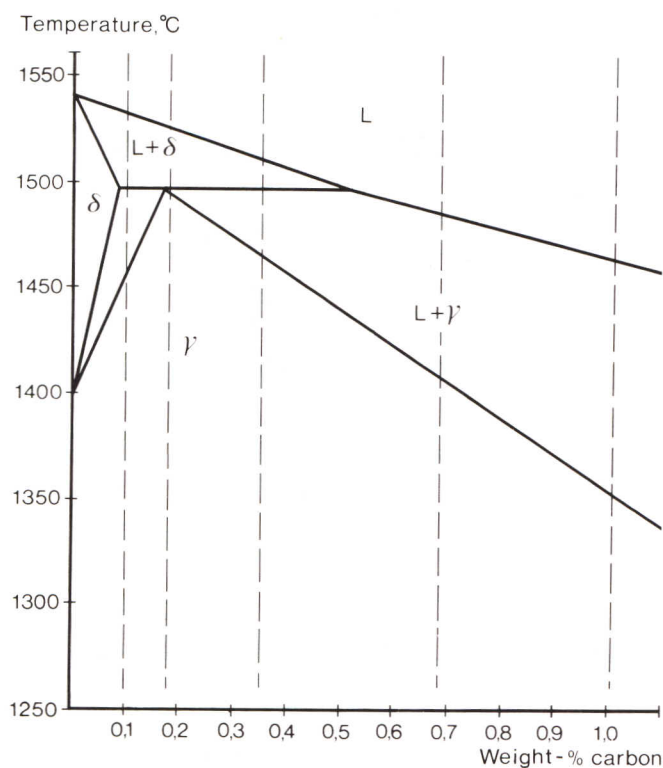


Figure 2.1 Fe-C system (After Metals Handbook, Vol 8, 1973, 275-276)

Low alloy steels usually contain modest amounts of chromium, nickel, molybdenum and vanadium for hardenability purposes. One of the elements may be present in concentrations of up to about 4%. In its effect on solidification carbon is still by far the most important element, so that these steels generally follow the behaviour shown in figure 2.1. The following commercial low alloy steels were studied:

No.	C	Si	Mn	Cr	Ni	Mo	V	%
208	0,10	0,3	0,6	1,2	3,2	0,1	—	
209	0,20	0,3	0,9	0,8	1,0	0,1	—	
210	0,27	0,02	0,3	1,7	3,5	0,4	0,1	
211	0,29	0,2	0,6	1,1	0,1	0,2	—	
212	0,30	0,2	0,5	1,0	3,2	0,3	—	
213	0,35	0,2	0,7	0,9	0,1	0,2	—	
214	0,52	0,2	0,9	1,1	0,1	—	—	
215	0,55	0,3	0,5	1,0	3,6	0,3	—	
216	1,01	0,2	0,3	1,6	—	—	—	

Table 2.2 Low alloy steels

References

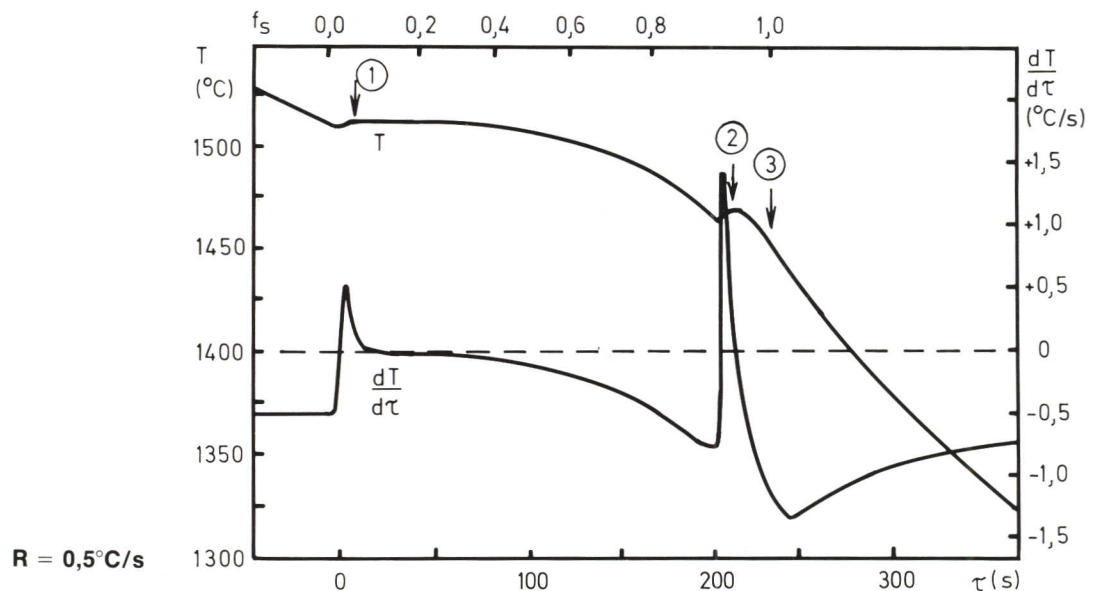
The solidification of carbon and low alloy steels has been investigated and described by many authors. Dendritic growth (kinetic aspects, arm spacings etc), has been studied in both laboratory ingots of varying sizes and in commercial ingots, [24–37]. Quantitative aspects of microsegregation have been discussed in references [24, 26, 30, 31, 32, 34, 35, 38–51]. Finally, references [52–54] are examples of papers which, while not predominantly concerned with dendritic growth or microsegregation, nevertheless contain information relevant to the solidification of carbon and low alloy steels.

STEEL 201. 0,1% CARBON STEEL**Designations**

SIS	AISI	Werkstoff Nr
1413	—	—

Composition (wt-%)

C	Si	Mn	P	S	Cr	Ni	Mo	Cu	Al _{tot}	N
0,11	0,12	1,25	0,040	0,018	0,06	0,03	0,07	0,07	0,038	0,012

Thermal Analysis

	Average Cooling Rate, R, ($^{\circ}\text{C/s}$)		
	2,0	0,5	0,1
Liquidus temperature, ferritic primary phase, $^{\circ}\text{C}$ ①	1513	1513	1515
Temperature of austenite formation, $^{\circ}\text{C}$ ②	1476	1476	1475
Solidus temperature, $^{\circ}\text{C}$ ③	1445	1450	1455
Solidification range, $^{\circ}\text{C}$	65	65	60
Solidification time, s	85	240	700

Precipitates

Interdendritic MnS.

Microsegregation

Element	Mn
I	1,3

$R = 0,5^{\circ}\text{C/s}$
 $T_q = 1390^{\circ}\text{C}$

Partly solidified

Figure 1

$R = 0,5^{\circ}\text{C/s}$

$T_q = 1510^{\circ}\text{C}$

$d = 65\ \mu\text{m}$

δ -dendrites and quenched liquid (L).

$\times 25$ 



Completely solidified

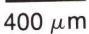
Figure 2

$R = 2,0^{\circ}\text{C/s}$

$T_q = 1390^{\circ}\text{C}$

$d = 80\ \mu\text{m}$

Figures 2–4: Former δ -dendrites, transformed to γ by the peritectic reaction.

$\times 25$ 

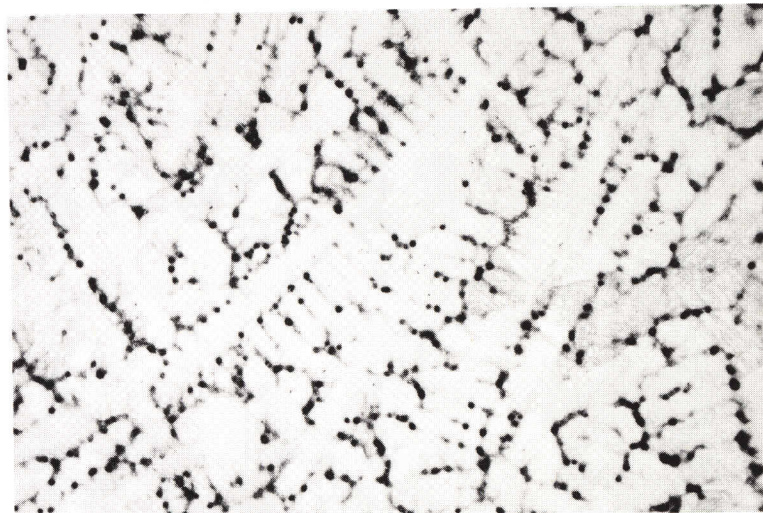


Figure 3

$R = 0,5^{\circ}\text{C/s}$

$T_q = 1390^{\circ}\text{C}$

$d = 130\ \mu\text{m}$

$\times 25$ 

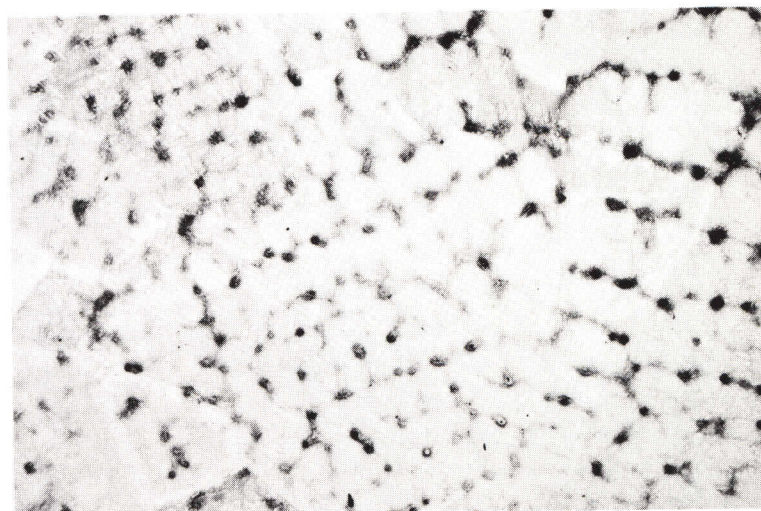
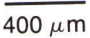


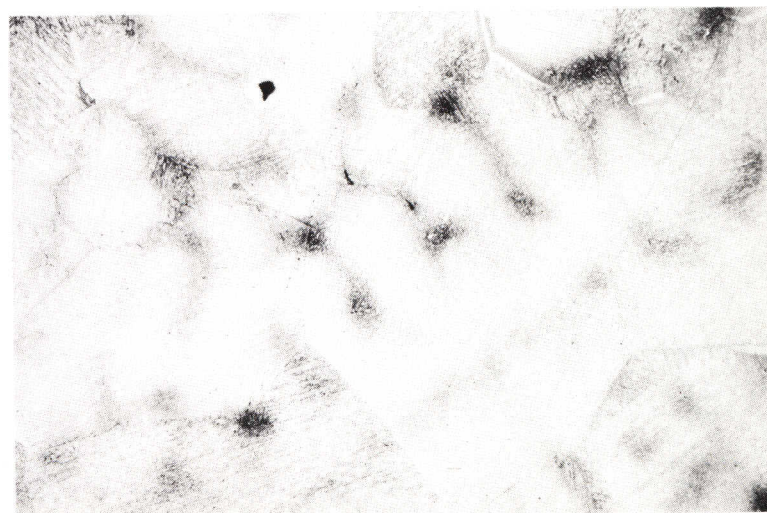
Figure 4

$R = 0,1^{\circ}\text{C/s}$

$T_q = 1390^{\circ}\text{C}$

$d = 300\ \mu\text{m}$

$\times 25$ 

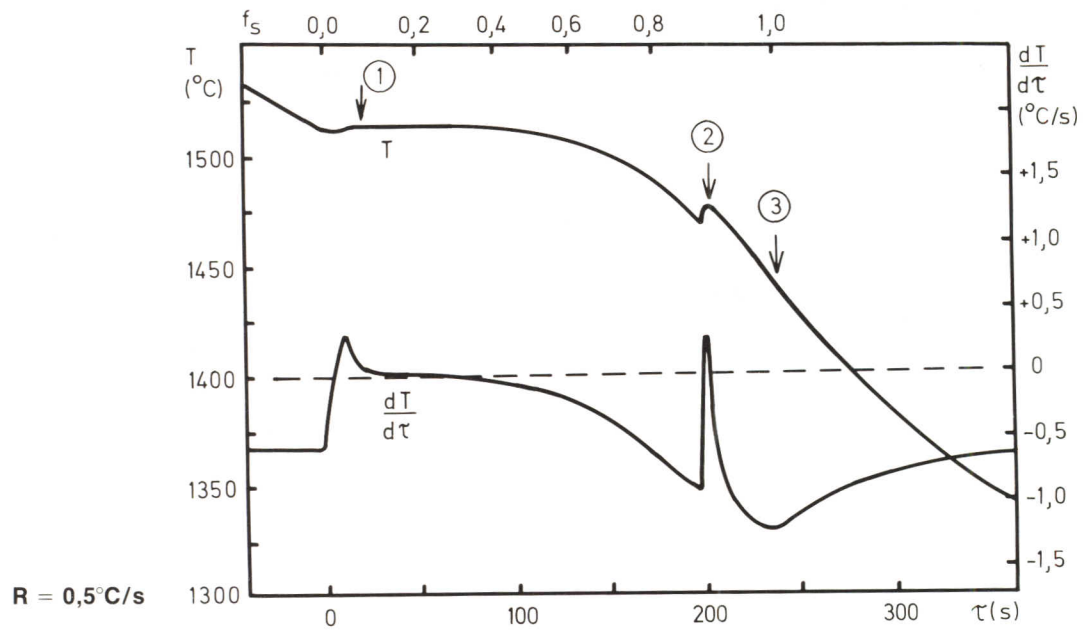


STEEL 202. 0,12 % CARBON STEEL**Designations**

SIS	AISI	Werkstoff Nr
–	–	1.0566

Composition (wt-%)

C	Si	Mn	P	S	Cr	Ni	Mo	Cu	Al _{tot}	Ce	N
0,12	0,27	1,53	0,010	0,005	0,02	0,03	<0,03	0,05	0,029	0,03	0,011

Thermal Analysis

Average Cooling Rate, R, (°C/s)

	2,0	0,5	0,1
Liquidus temperature, ferritic primary phase, °C (1)	1514	1515	1514
Temperature of austenite formation, °C (2)	1471	1475	1477
Solidus temperature, °C (3)	1440	1440	1460
Solidification range, °C	75	75	55
Solidification time, s	105	230	700

Precipitates

Globular rare earth inclusions from addition of Rare Earth Metals (REM).

Microsegregation

Element	Mn
I	1,4

R = 0,5 °C/s
T_q = 1390 °C

Partly solidified

Figure 1

$R = 0,5^{\circ}\text{C/s}$

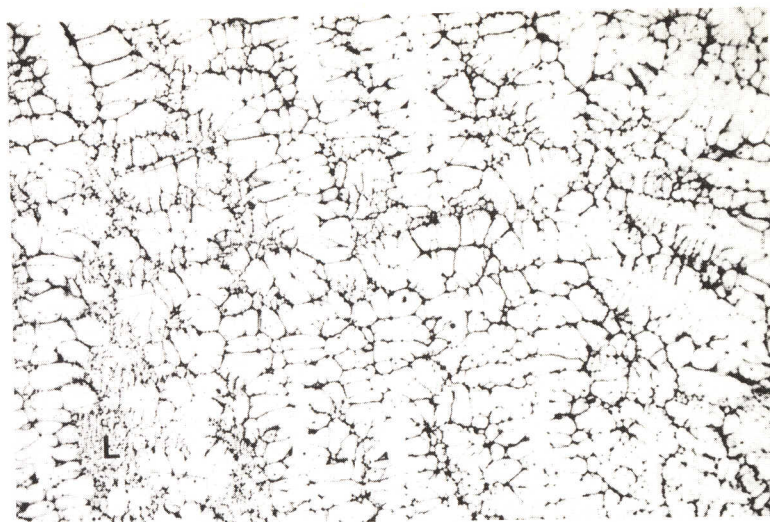
$T_q = 1510^{\circ}\text{C}$

$d = 70\ \mu\text{m}$

δ -dendrites and quenched liquid (L).

$\times 25$

400 μm



Completely solidified

Figure 2

$R = 2,0^{\circ}\text{C/s}$

$T_q = 1390^{\circ}\text{C}$

$d = 85\ \mu\text{m}$

Figures 2–4: Former δ -dendrites, transformed to γ by the peritectic reaction.

$\times 25$

400 μm

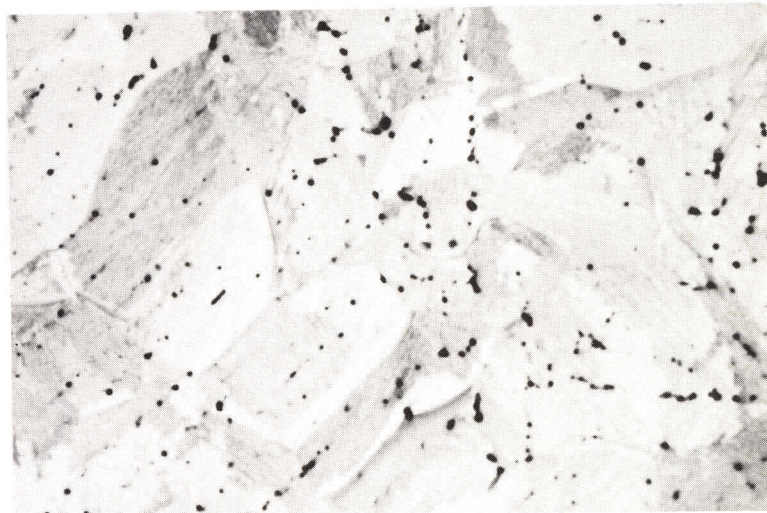


Figure 3

$R = 0,5^{\circ}\text{C/s}$

$T_q = 1390^{\circ}\text{C}$

$d = 200\ \mu\text{m}$

$\times 25$

400 μm



Figure 4

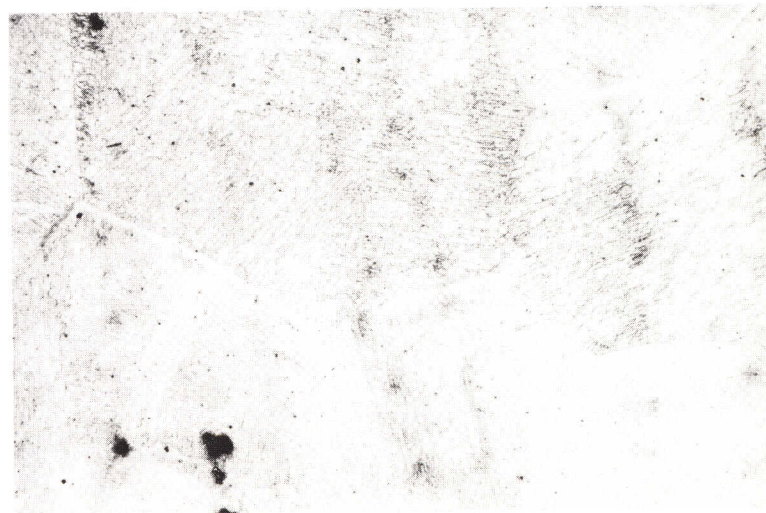
$R = 0,1^{\circ}\text{C/s}$

$T_q = 1390^{\circ}\text{C}$

$d = 390\ \mu\text{m}$

$\times 25$

400 μm



STEEL 203. 0,18 % CARBON STEEL

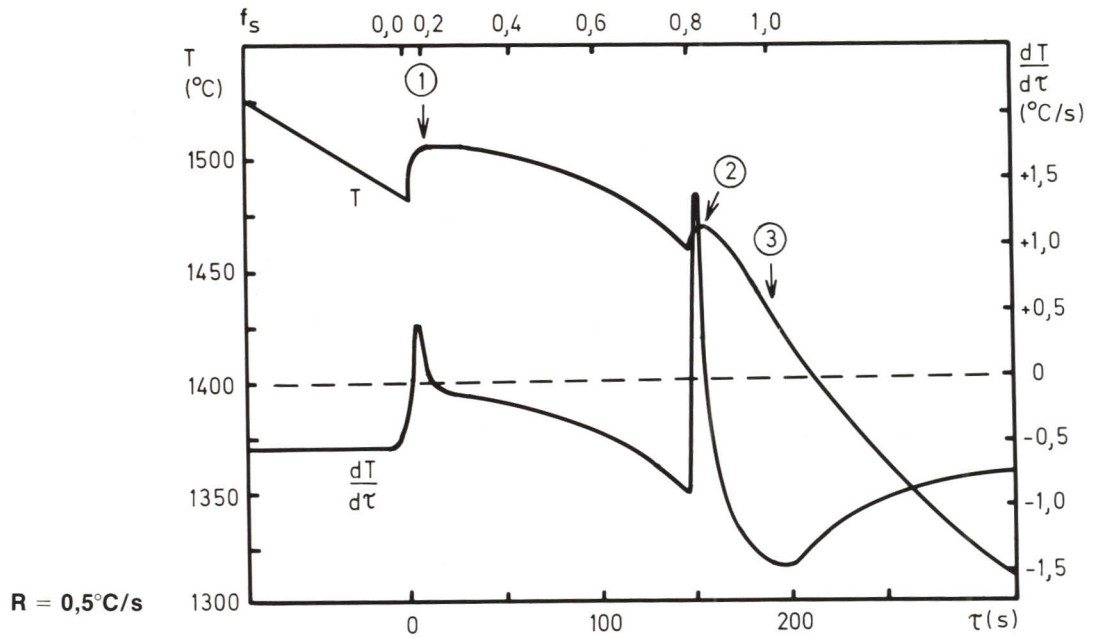
Designations

SIS	AISI	Werkstoff Nr
2106	—	—

Composition (wt-%)

C	Si	Mn	P	S	Cr	Ni	Mo	Cu	Nb	Al _{tot}	N
0,18	0,44	1,26	0,016	0,025	0,01	0,02	0,06	0,02	0,03	0,004	0,007

Thermal Analysis



	Average Cooling Rate, R, (°C/s)		
	2,0	0,5	0,1
Liquidus temperature, ferritic primary phase, °C ①	1507	1506	1507
Temperature of austenite formation, °C ②	1467	1470	1473
Solidus temperature, °C ③	1415	1430	1460
Solidification range, °C	90	80	50
Solidification time, s	85	210	570

Precipitates

Interdendritic MnS.

Microsegregation

Element	Mn
I	1,4

R = 0,5 °C/s
T_q = 1370 °C

Partly solidified

Figure 1

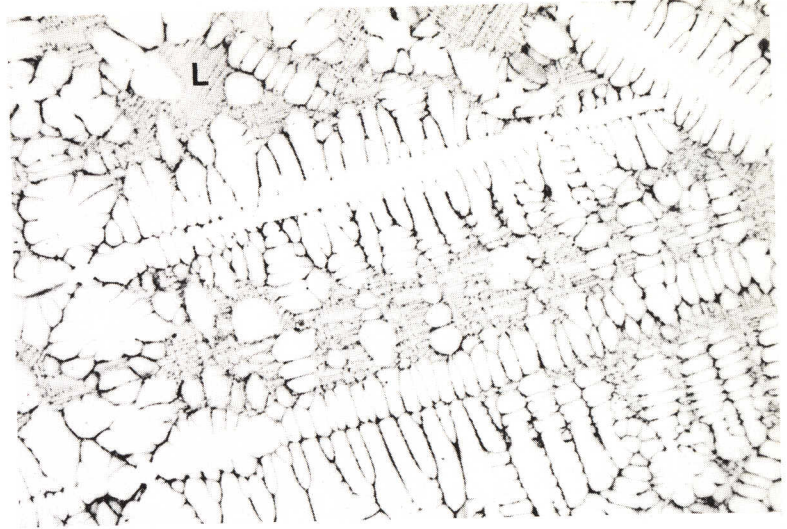
R = 0,5°C/s

T_q = 1500°C

d = 65 μm

δ-dendrites and quenched liquid (L).

× 25 



Completely solidified

Figure 2

R = 2,0°C/s

T_q = 1370°C

d = 80 μm

Figures 2–4: Former δ-dendrites, transformed to γ by the peritectic reaction.

× 25 

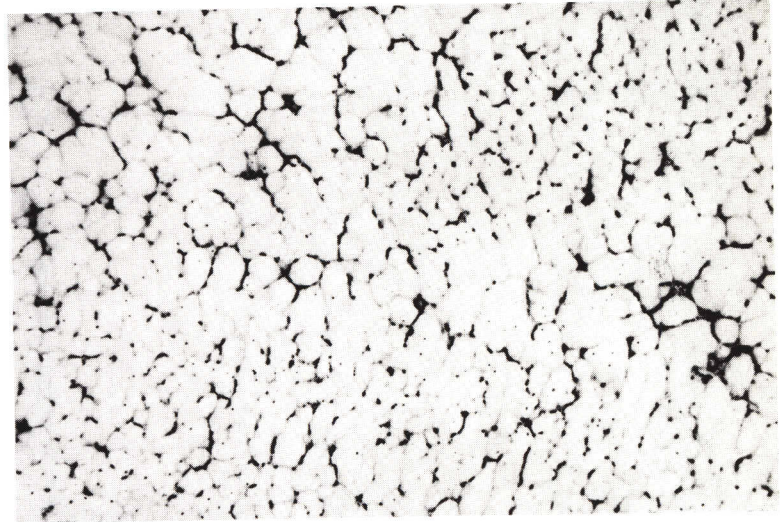


Figure 3

R = 0,5°C/s

T_q = 1370°C

d = 190 μm

× 25 

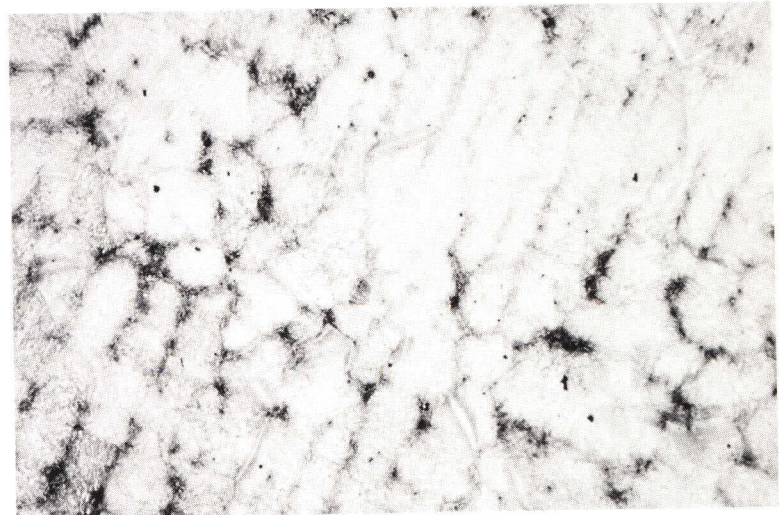
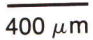


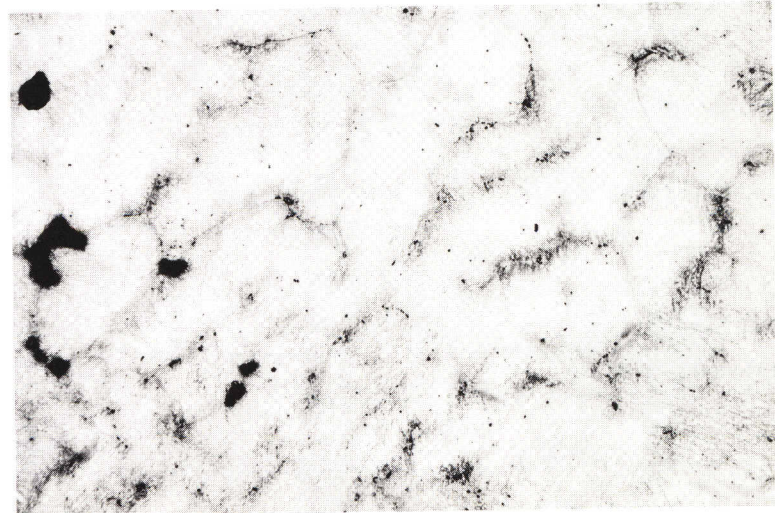
Figure 4

R = 0,1°C/s

T_q = 1370°C

d = 250 μm

× 25 



STEEL 204. 0,2% CARBON STEEL

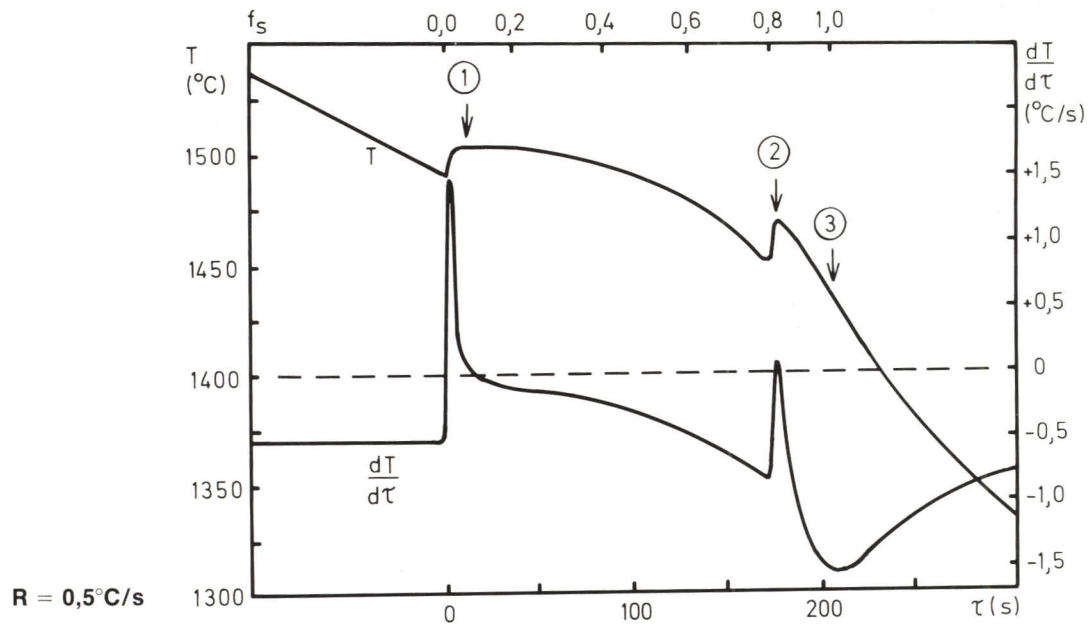
Designations

SIS	AISI	Werkstoff Nr
2172	—	1.0580

Composition (wt-%)

C	Si	Mn	P	S	Cr	Ni	Mo	Cu	Al _{tot}	N
0,19	0,40	1,42	0,012	0,007	0,07	0,13	0,02	0,08	0,006	0,005

Thermal Analysis



	Average Cooling Rate, R, (°C/s)		
	2,0	0,5	0,1
Liquidus temperature, ferritic primary phase, °C ①	1503	1503	1506
Temperature of austenite formation, °C ②	1480	1477	1480
Solidus temperature, °C ③	1425	1440	1460
Solidification range, °C	85	65	45
Solidification time, s	80	210	600

Precipitates

Interdendritic MnS.

Microsegregation

Element	Mn
I	1,6

R = 0,5 °C/s
T_q = 1370 °C

Partly solidified

Figure 1

$R = 0,5^{\circ}\text{C/s}$

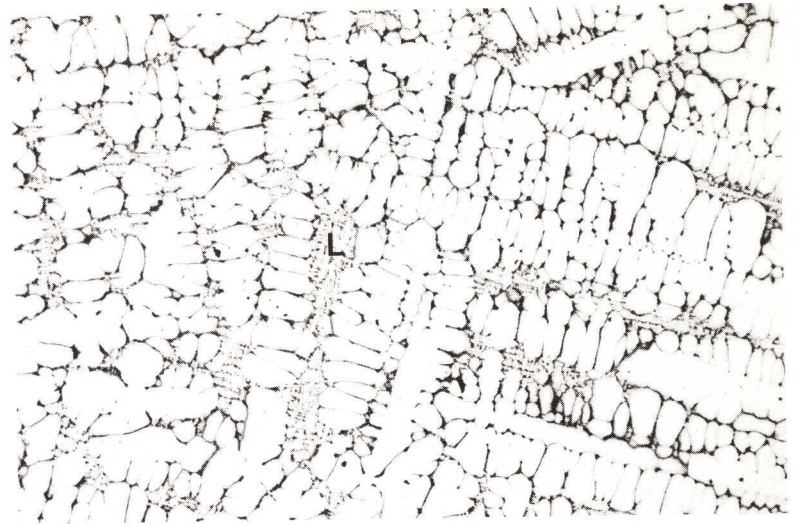
$T_q = 1498^{\circ}\text{C}$

$d = 85 \mu\text{m}$

δ -dendrites and quenched liquid (L).

$\times 25$

400 μm



Completely solidified

Figure 2

$R = 2,0^{\circ}\text{C/s}$

$T_q = 1370^{\circ}\text{C}$

$d = 75 \mu\text{m}$

Figures 2–4: Former δ -dendrites, transformed to γ by the peritectic reaction.

$\times 25$

400 μm



Figure 3

$R = 0,5^{\circ}\text{C/s}$

$T_q = 1370^{\circ}\text{C}$

$d = 120 \mu\text{m}$

$\times 25$

400 μm

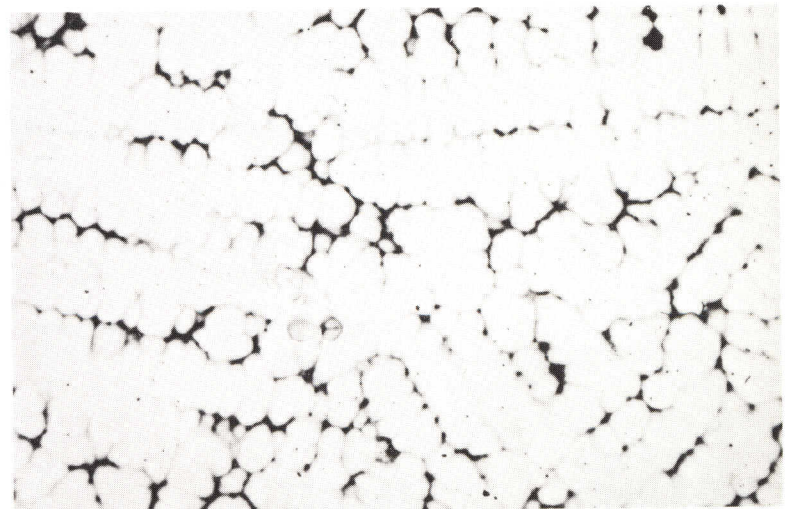


Figure 4

$R = 0,1^{\circ}\text{C/s}$

$T_q = 1370^{\circ}\text{C}$

$d = 230 \mu\text{m}$

$\times 25$

400 μm



STEEL 205. 0,4 % CARBON STEEL

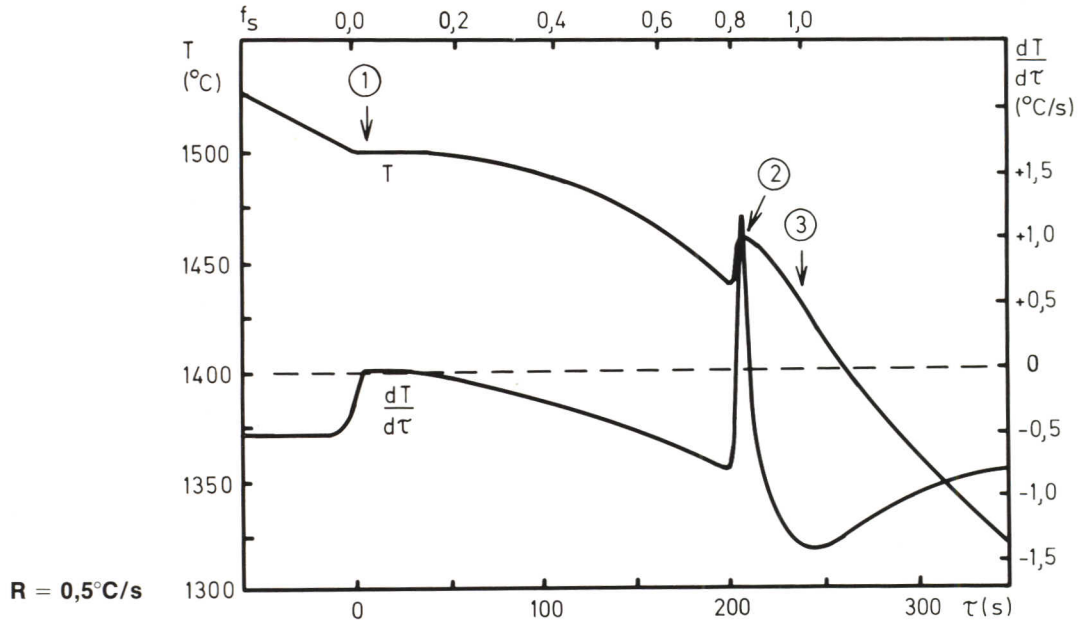
Designations

SIS	AISI	Werkstoff Nr
1550	1034	1.1181

Composition (wt-%)

C	Si	Mn	P	S	Cr	Ni	Mo	Cu	Al _{tot}	N
0,36	0,27	0,58	0,015	0,012	0,08	0,05	0,02	0,12	0,004	0,007

Thermal Analysis



	Average Cooling Rate, R , ($^\circ\text{C/s}$)		
	2,0	0,5	0,1
Liquidus temperature, ferritic primary phase, $^\circ\text{C}$ (1)	1496	1498	1501
Temperature of austenite formation, $^\circ\text{C}$ (2)	1479	1480	1483
Solidus temperature, $^\circ\text{C}$ (3)	1415	1425	1440
Solidification range, $^\circ\text{C}$	85	75	60
Solidification time, s	85	230	840

Precipitates

Interdendritic MnS.

Microsegregation

Element	Mn
I	1,6

$R = 0,5^\circ\text{C/s}$
 $T_q = 1370^\circ\text{C}$

Partly solidified

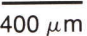
Figure 1

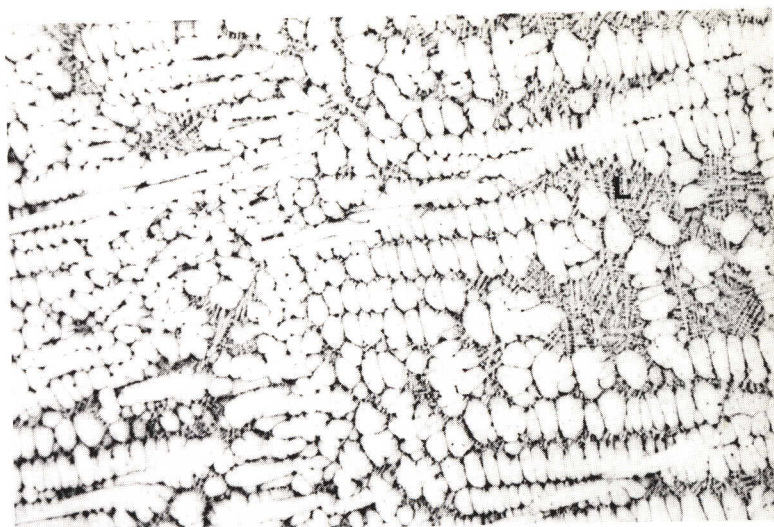
R = 0,5°C/s

T_q = 1480°C

d = 50 μm

δ-dendrites and quenched liquid (L).

× 25 



Completely solidified

Figure 2

R = 2,0°C/s

T_q = 1370°C

d = 85 μm

Figures 2–4: Former δ-dendrites, transformed to γ by the peritectic reaction.

× 25 

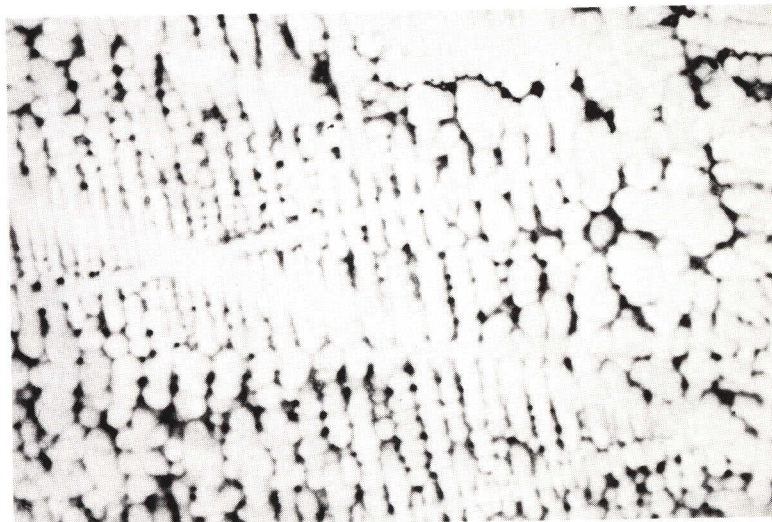


Figure 3

R = 0,5°C/s

T_q = 1370°C

d = 90 μm

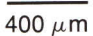
× 25 



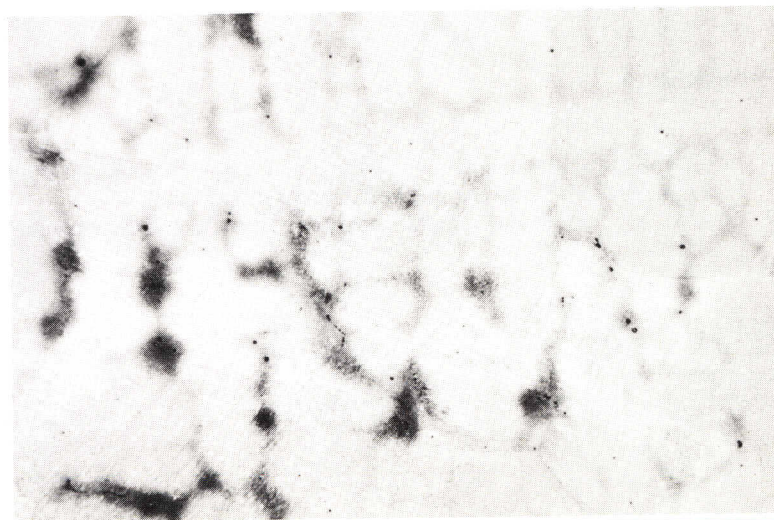
Figure 4

R = 0,1°C/s

T_q = 1370°C

d = 280 μm

× 25 



STEEL 206. 0,7 % CARBON STEEL

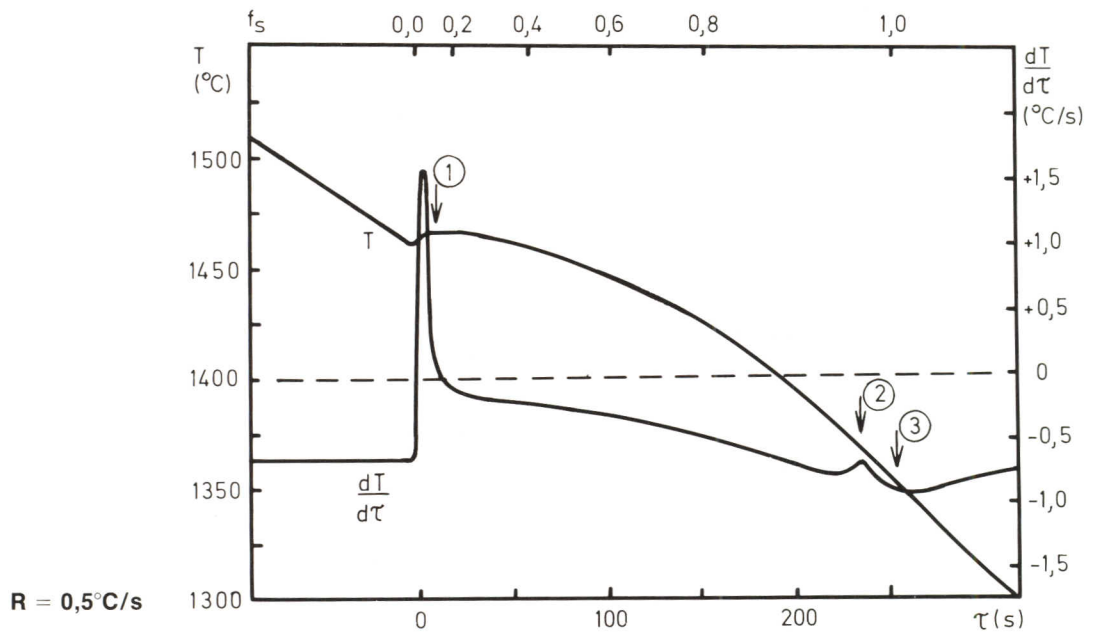
Designations

SIS	AISI	Werkstoff Nr
1770	1070	1.1231

Composition (wt-%)

C	Si	Mn	P	S	Cr	Ni	Mo	Cu	Al _{tot}	N
0,69	0,23	0,72	0,022	0,024	0,02	0,02	0,01	0,03	0,006	0,002

Thermal Analysis



	Average Cooling Rate, R, ($^\circ\text{C/s}$)		
	2,0	0,5	0,1
Liquidus temperature, austenitic primary phase, $^\circ\text{C}$ ①	1471	1466	1474
Temperature of formation of eutectic, $^\circ\text{C}$ ②	1370 – 1335	1370 – 1355	1420 – 1370
Solidus temperature, $^\circ\text{C}$ ③	1335	1355	1370
Solidification range, $^\circ\text{C}$	140	120	105
Solidification time, s	105	250	1020

Precipitates

1. Interdendritic $\text{Fe}_3\text{P} - \text{Fe}_3\text{C} - \text{austenite}$ eutectic. The eutectic remained after cooling to 850°C , (see figures 9 and 10), but was dissolved after homogenizing for 4 h at 1200°C .
2. MnS. (Distribution and morphology at different cooling rates shown in figures 5 – 8.)

Microsegregation

Element	Mn
I	1,7

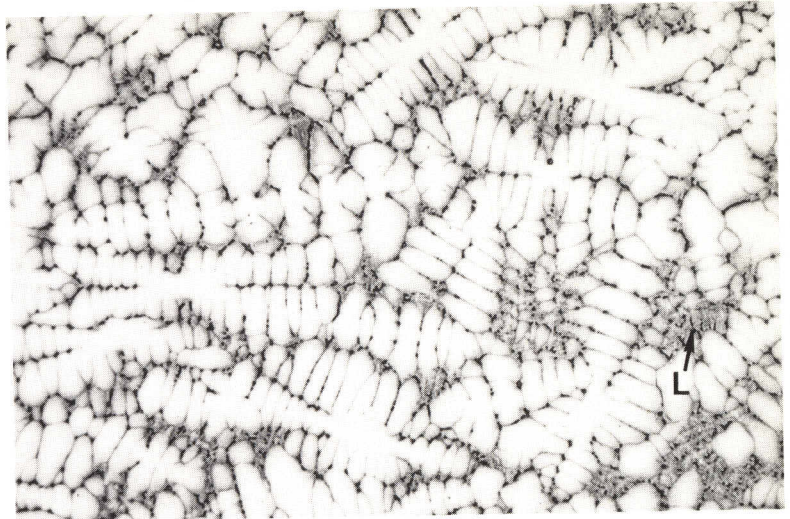
$R = 0,5^\circ\text{C/s}$
 $T_q = 1300^\circ\text{C}$

Partly solidified

Figure 1

$R = 0,5^{\circ}\text{C/s}$
 $T_q = 1455^{\circ}\text{C}$
 $d = 70 \mu\text{m}$
 γ -dendrites and quenched liquid (L).

$\times 25$ 



Completely solidified

Figure 2

$R = 2,0^{\circ}\text{C/s}$
 $T_q = 1300^{\circ}\text{C}$
 $d = 75 \mu\text{m}$
 Figures 2–4: γ -dendrites.

$\times 25$ 

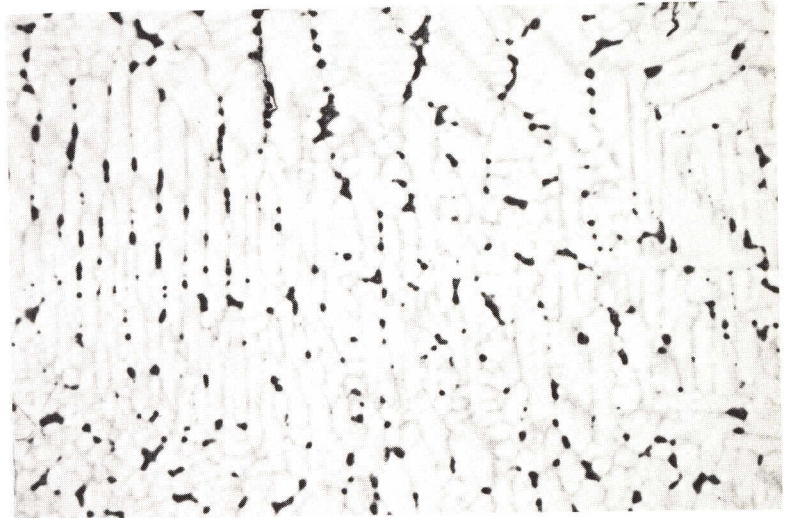
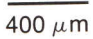


Figure 3

$R = 0,5^{\circ}\text{C/s}$
 $T_q = 1300^{\circ}\text{C}$
 $d = 130 \mu\text{m}$

$\times 25$ 

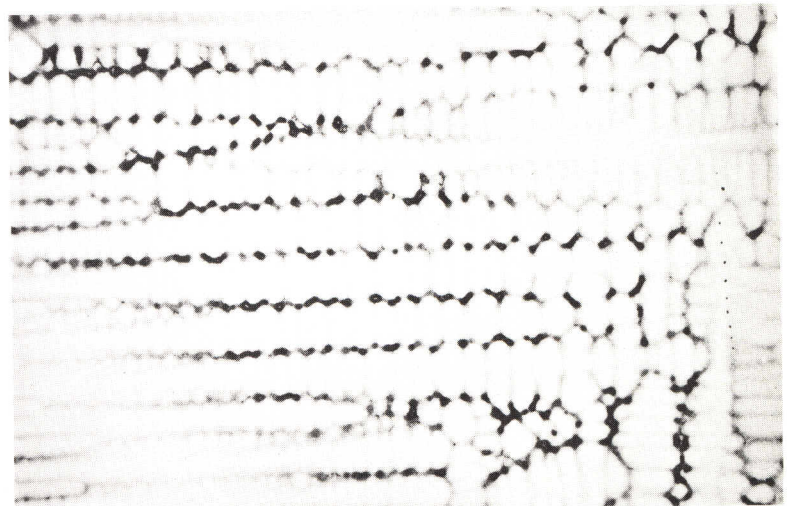
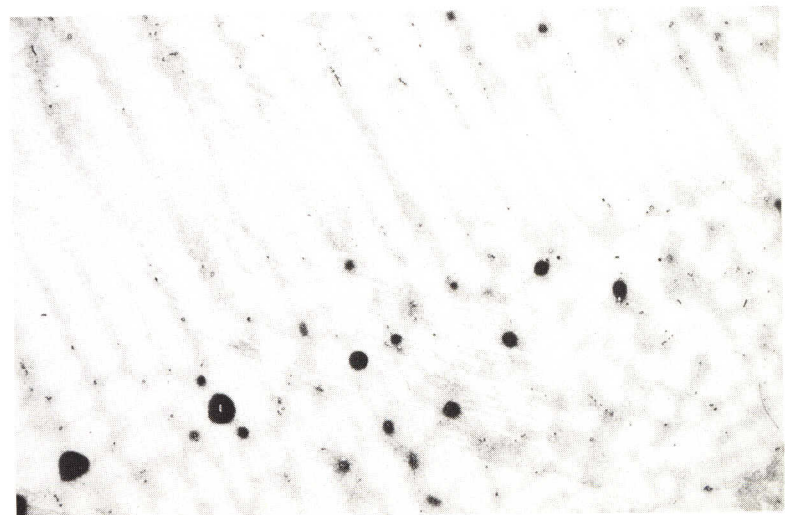


Figure 4

$R = 0,1^{\circ}\text{C/s}$
 $T_q = 1300^{\circ}\text{C}$
 $d = 160 \mu\text{m}$

$\times 25$ 



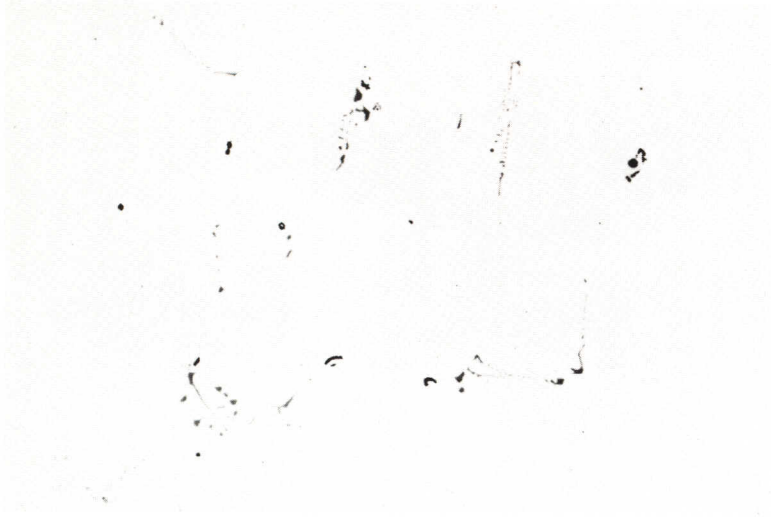


Figure 5
R = 0,5°C/s
Tq = 1300°C
Interdendritic MnS.

100 μm \times 150

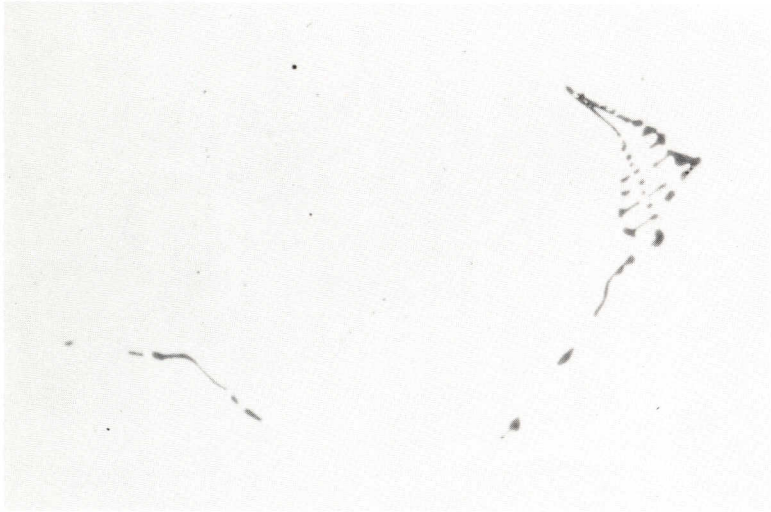


Figure 6
R = 2,0°C/s
Tq = 1300°C
Figures 6–8 show the influence of cooling rate on manganese sulphide coarseness.

25 μm \times 600



Figure 7
R = 0,5°C/s
Tq = 1300°C

25 μm \times 600

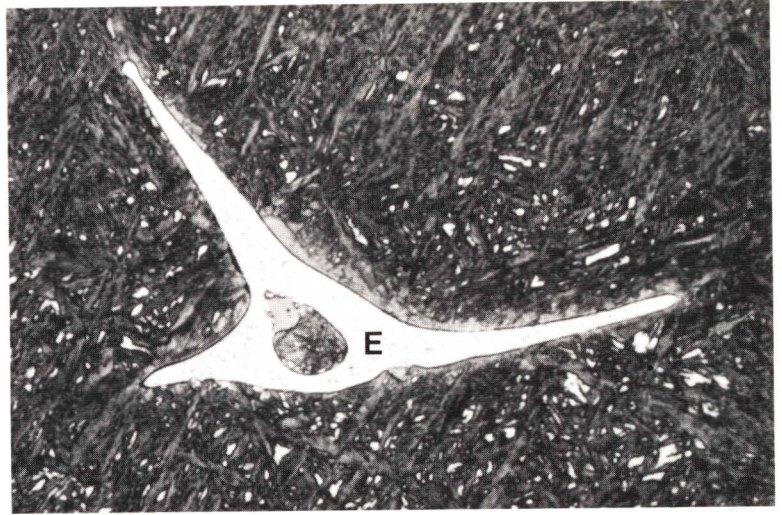


Figure 8
R = 0,1°C/s
Tq = 1300°C

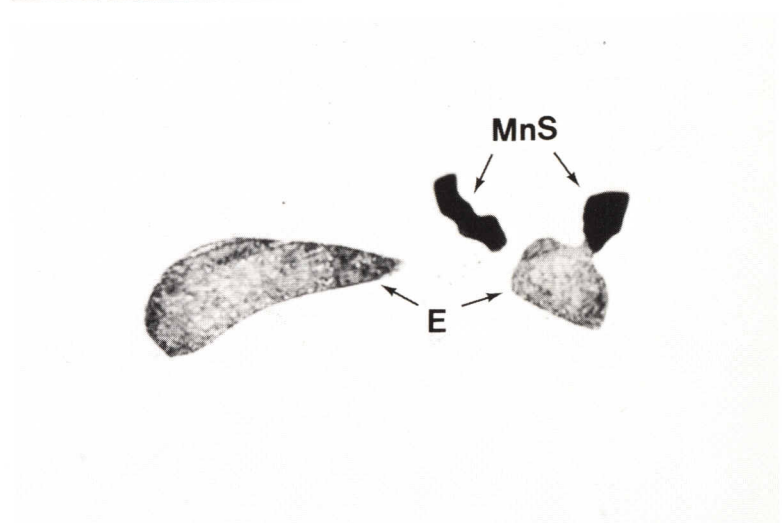
25 μm \times 600

Figure 9

R = 0,5°C/s

T_q = 1300°CFigures 9–10: Interdendritic Fe₃P-Fe₃C-austenite eutectic (E), approximately 0,05 vol-%.× 1000 10 μm**Figure 10**

R = 2,0°C/s

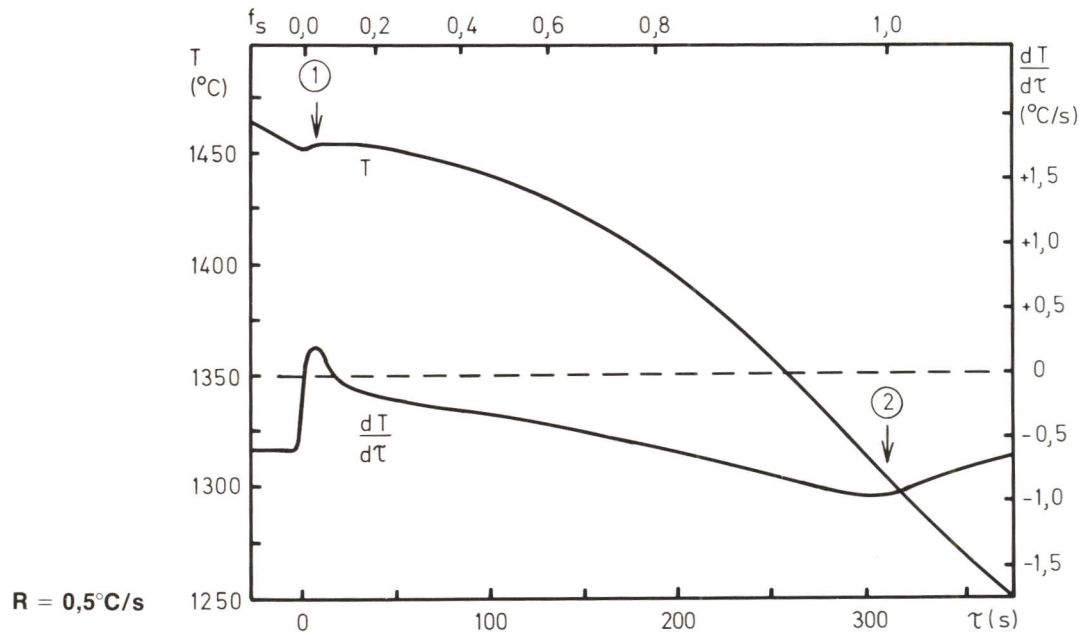
T_q = 800°CEtched to darken and confirm the existence of the Fe₃P phase in the eutectic (E). The eutectic contains 2 wt-% P.× 2000 5 μm

STEEL 207. 1,0 % CARBON STEEL**Designations**

SIS	AISI	Werkstoff Nr
1870	1095	1.1274

Composition (wt-%)

C	Si	Mn	P	S	Cr	Ni	Mo	Cu	Al _{tot}	N
1,01	0,25	0,46	0,012	0,009	0,02	0,03	0,02	0,03	≤0,004	0,002

Thermal Analysis**Average Cooling Rate, R, (°C/s)**

	2,0	0,5	0,1
Liquidus temperature, austenitic primary phase, °C (1)	1457	1457	1459
Solidus temperature, °C (2)	1310	1320	1340
Solidification range, °C	150	140	120
Solidification time, s	110	300	1600

Precipitates

- MnS
- Interdendritic eutectic (< 0,05 vol. %), as in steel 206

Microsegregation

Element	Mn
I	2,1

$R = 0,5^\circ\text{C/s}$
 $T_q = 1260^\circ\text{C}$

Partly solidified

Figure 1

$R = 0,5^{\circ}\text{C/s}$

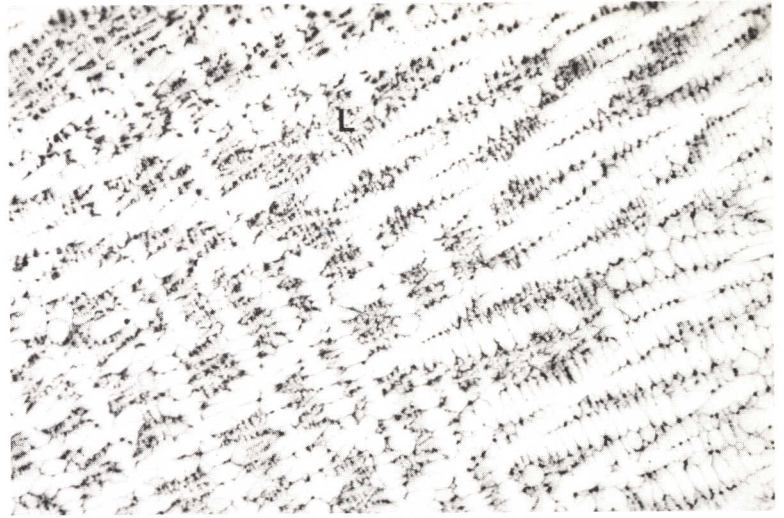
$T_q = 1445^{\circ}\text{C}$

$d = 50\ \mu\text{m}$

γ -dendrites and quenched liquid (L).

$\times 25$

$\overline{\hspace{1cm}}$
400 μm



Completely solidified

Figure 2

$R = 2,0^{\circ}\text{C/s}$

$T_q = 1260^{\circ}\text{C}$

$d = 70\ \mu\text{m}$

Figures 2–4: γ -dendrites.

$\times 25$

$\overline{\hspace{1cm}}$
400 μm

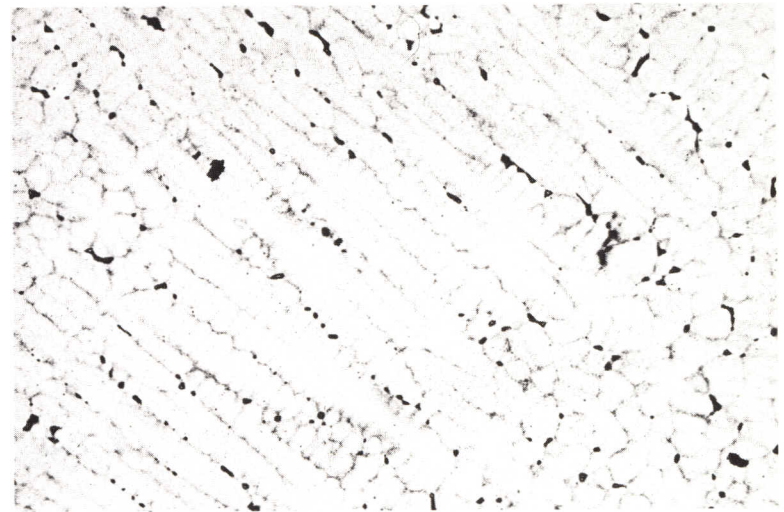


Figure 3

$R = 0,5^{\circ}\text{C/s}$

$T_q = 1260^{\circ}\text{C}$

$d = 80\ \mu\text{m}$

$\times 25$

$\overline{\hspace{1cm}}$
400 μm

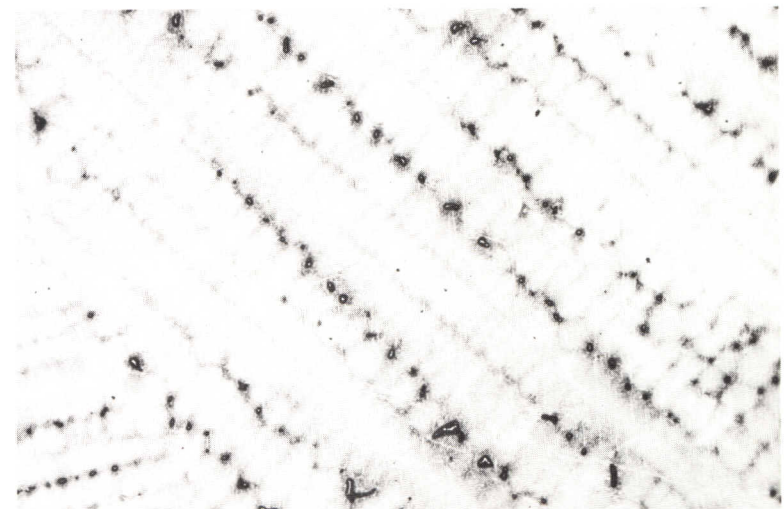


Figure 4

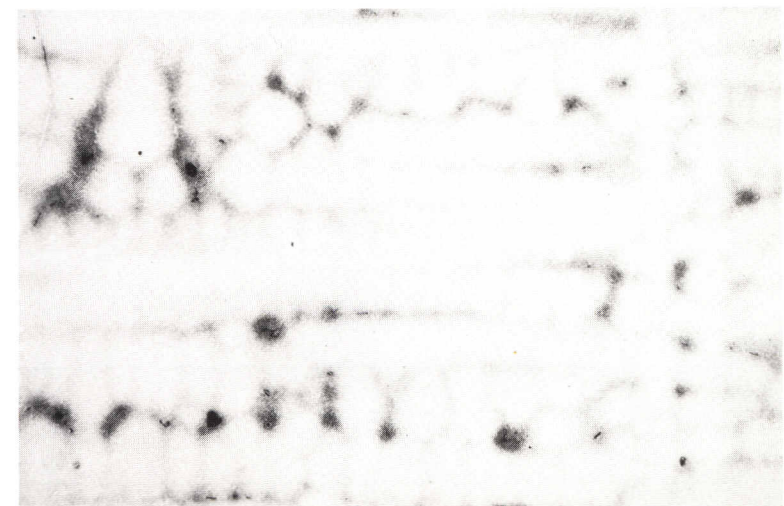
$R = 0,1^{\circ}\text{C/s}$

$T_q = 1260^{\circ}\text{C}$

$d = 210\ \mu\text{m}$

$\times 25$

$\overline{\hspace{1cm}}$
400 μm



STEEL 208. 0,1% C Cr Ni LOW ALLOY STEEL

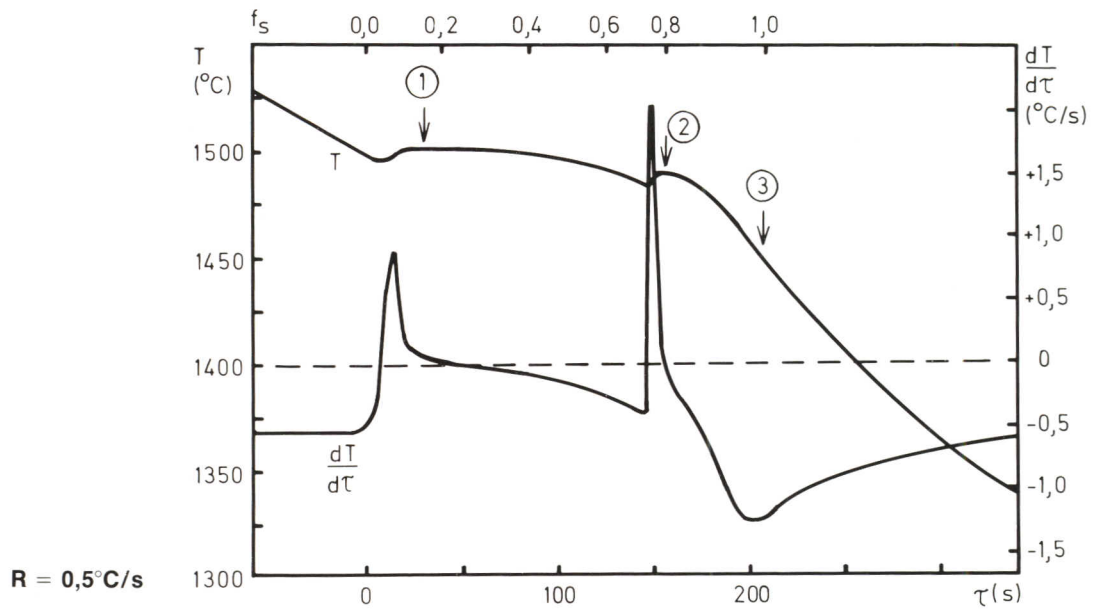
Designations

SIS	AISI	Werkstoff Nr
—	9310	—

Composition (wt-%)

C	Si	Mn	P	S	Cr	Ni	Mo	Cu	V	Al _{tot}	N
0,10	0,28	0,57	0,008	0,009	1,14	3,3	0,14	0,11	0,02	0,013	0,009

Thermal Analysis



	Average Cooling Rate, R, (°C/s)		
	2,0	0,5	0,1
Liquidus temperature, ferritic primary phase, °C ①	1501	1501	1502
Temperature of austenite formation, °C ②	1485	1485	1487
Solidus temperature, °C ③	1450	1450	1465
Solidification range, °C	50	50	40
Solidification time, s	85	210	640

Precipitates

—

Microsegregation

Element	Cr	Ni	Mo
I	1,3	1,4	2,5

R = 0,5 °C/s
T_q = 1400 °C

Partly solidified

Figure 1

$R = 0,5^{\circ}\text{C/s}$

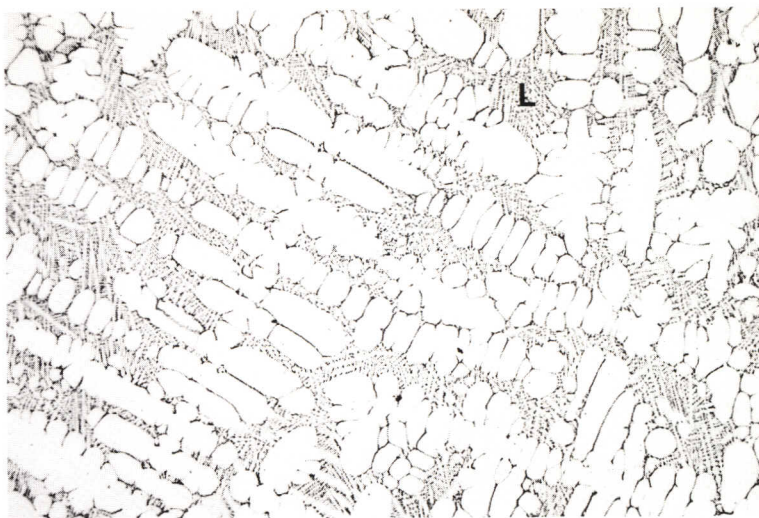
$T_q = 1495^{\circ}\text{C}$

$d = 70\ \mu\text{m}$

δ -dendrites and quenched liquid (L).

$\times 25$

400 μm



Completely solidified

Figure 2

$R = 2,0^{\circ}\text{C/s}$

$T_q = 1400^{\circ}\text{C}$

$d = 75\ \mu\text{m}$

Figures 2–4: Former δ -dendrites, transformed to γ by the peritectic reaction.

$\times 25$

400 μm

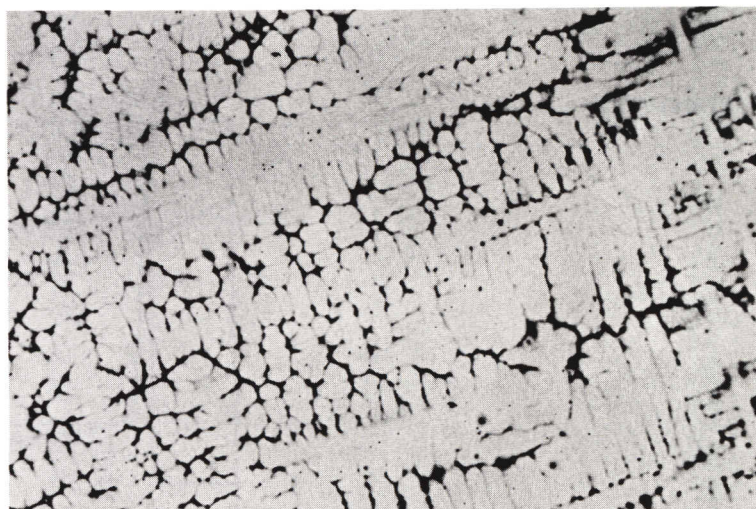


Figure 3

$R = 0,5^{\circ}\text{C/s}$

$T_q = 1400^{\circ}\text{C}$

$d = 110\ \mu\text{m}$

$\times 25$

400 μm

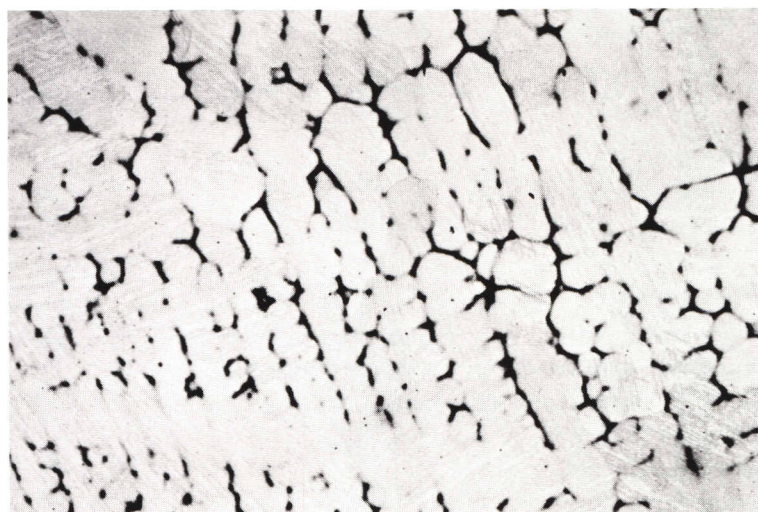


Figure 4

$R = 0,1^{\circ}\text{C/s}$

$T_q = 1400^{\circ}\text{C}$

$d = 250\ \mu\text{m}$

$\times 25$

400 μm

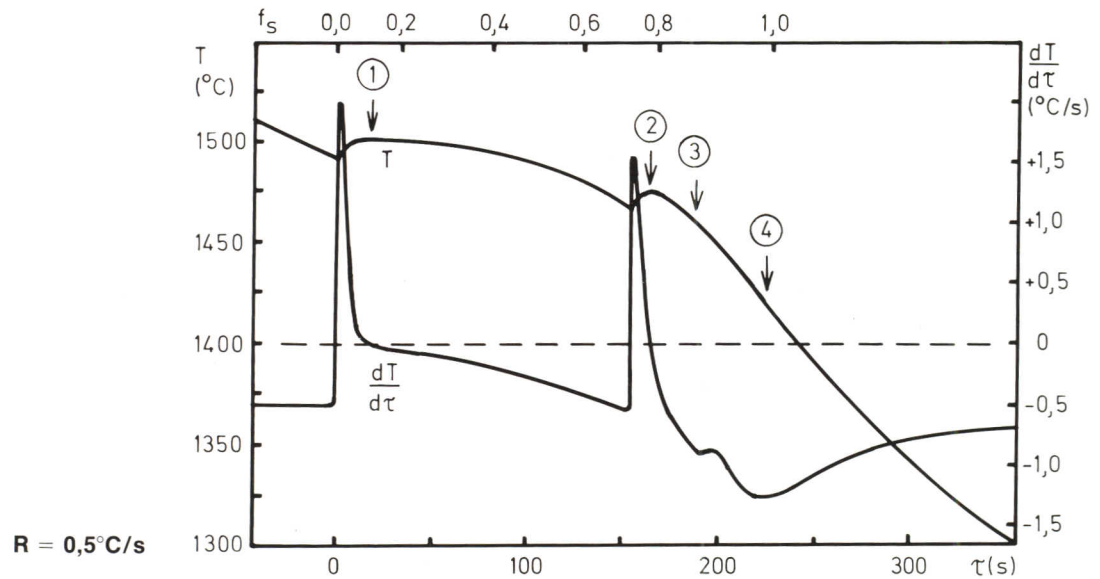


STEEL 209. 0,2% C Cr Ni LOW ALLOY STEEL**Designations**

SIS	AISI	Werkstoff Nr
2512	–	–

Composition (wt-%)

C	Si	Mn	P	S	Cr	Ni	Mo	Cu	V	Al _{tot}	N
0,20	0,25	0,90	0,014	0,039	0,81	1,05	0,06	0,07	0,02	0,036	0,009

Thermal Analysis**Average Cooling Rate, R, (°C/s)**

	2,0	0,5	0,1
Liquidus temperature, ferritic primary phase, °C (1)	1502	1502	1503
Temperature of austenite formation, °C (2)	1474	1474	1465
Temperature of MnS-formation, °C (3)	1460 – 1420	1460 – 1425	– 1445
Solidus temperature, °C (4)	1420	1425	1445
Solidification range, °C	85	80	60
Solidification time, s	95	230	750

Precipitates

MnS. The steel was resulphurized (see figures 5 – 7).

Microsegregation

Element	Cr	Ni
I	1,5	1,4

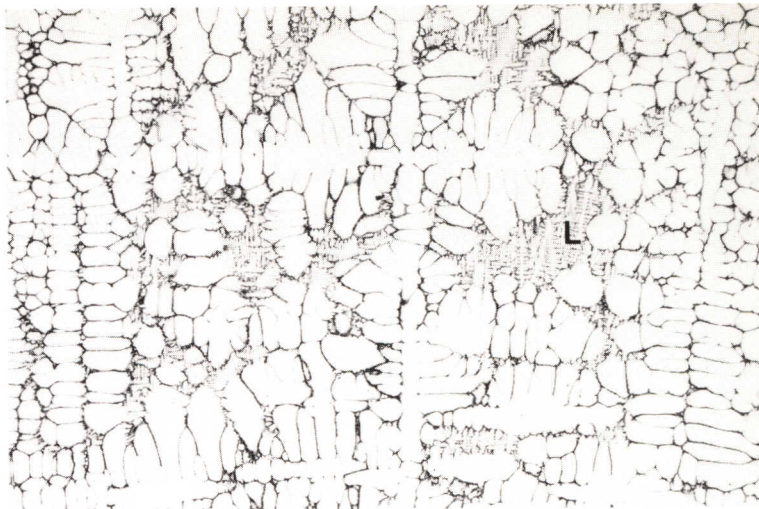
R = 0,5 °C/s
T_q = 1370 °C

Partly solidified

Figure 1

R = 0,5°C/s
 T_q = 1495°C
 d = 60 μm
 δ-dendrites and quenched liquid (L).

× 25 400 μm



Completely solidified

Figure 2

R = 2,0°C/s
 T_q = 1370°C
 d = 85 μm
 Figures 2–4: Former δ-dendrites,
 transformed to γ by the peritectic reaction.

× 25 400 μm

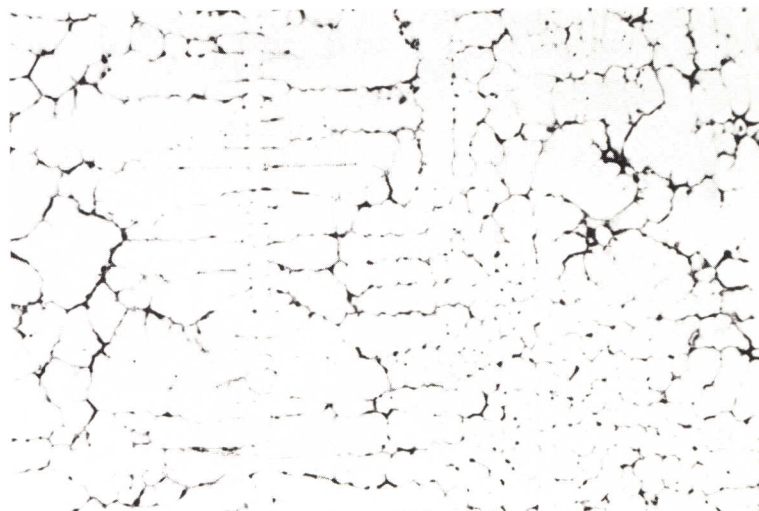


Figure 3

R = 0,5°C/s
 T_q = 1370°C
 d = 110 μm

× 25 400 μm

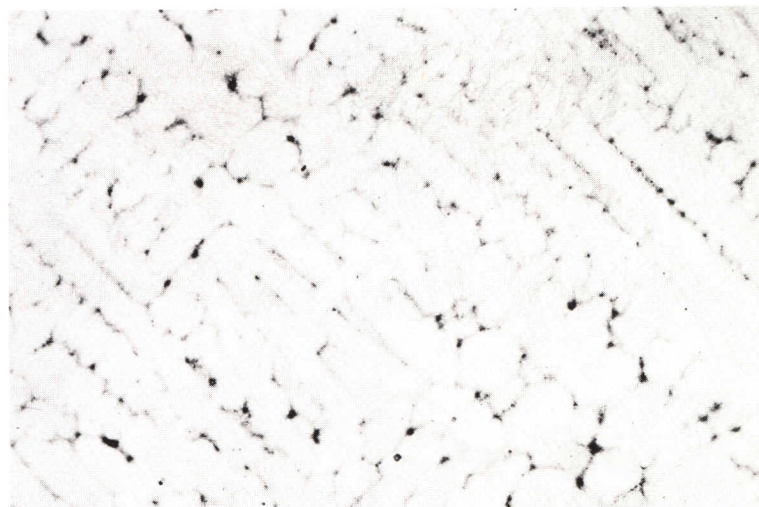


Figure 4

R = 0,1°C/s
 T_q = 1370°C
 d = 180 μm

× 25 400 μm

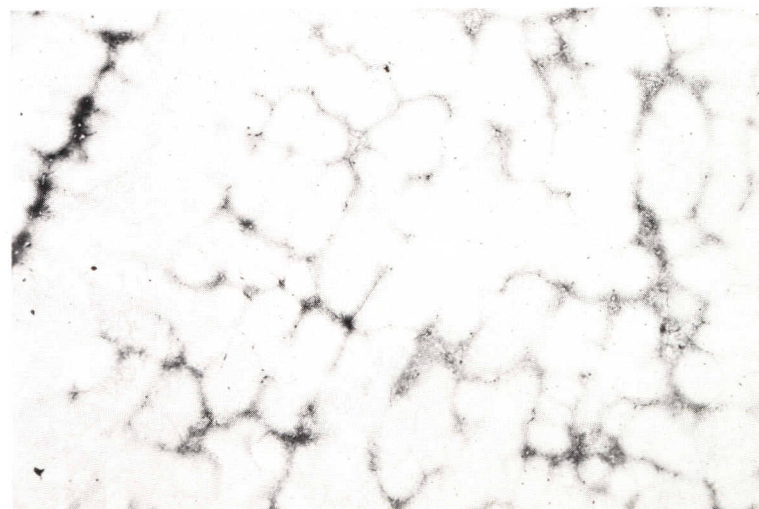




Figure 5

R = 2,0°C/s

T_q = 1370°C

Figures 5–7: Interdentritic MnS.

100 μm × 150

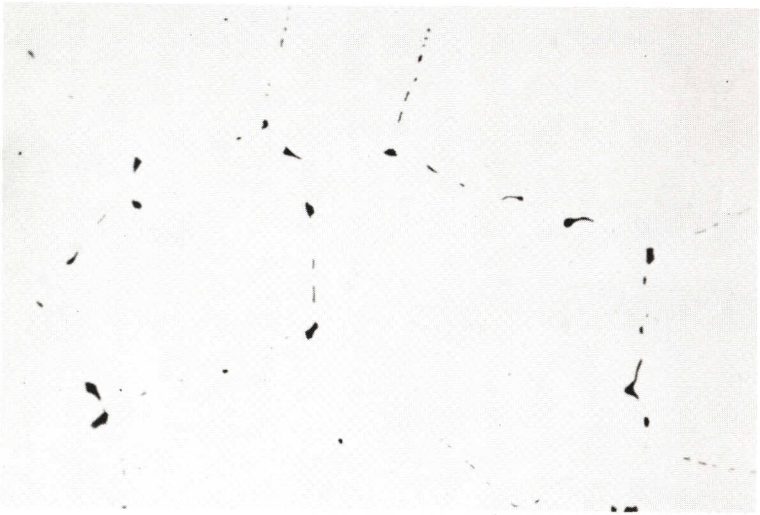


Figure 6

R = 0,1°C/s

T_q = 1370°C

100 μm × 150

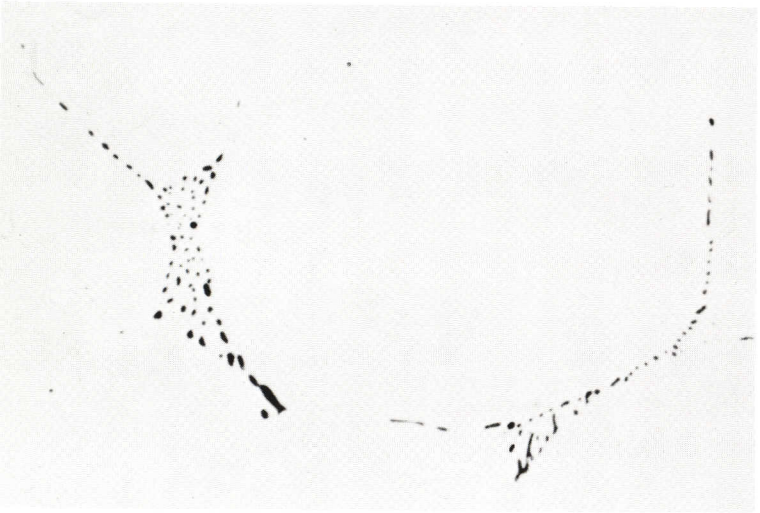


Figure 7

R = 2,0°C/s

T_q = 1370°C

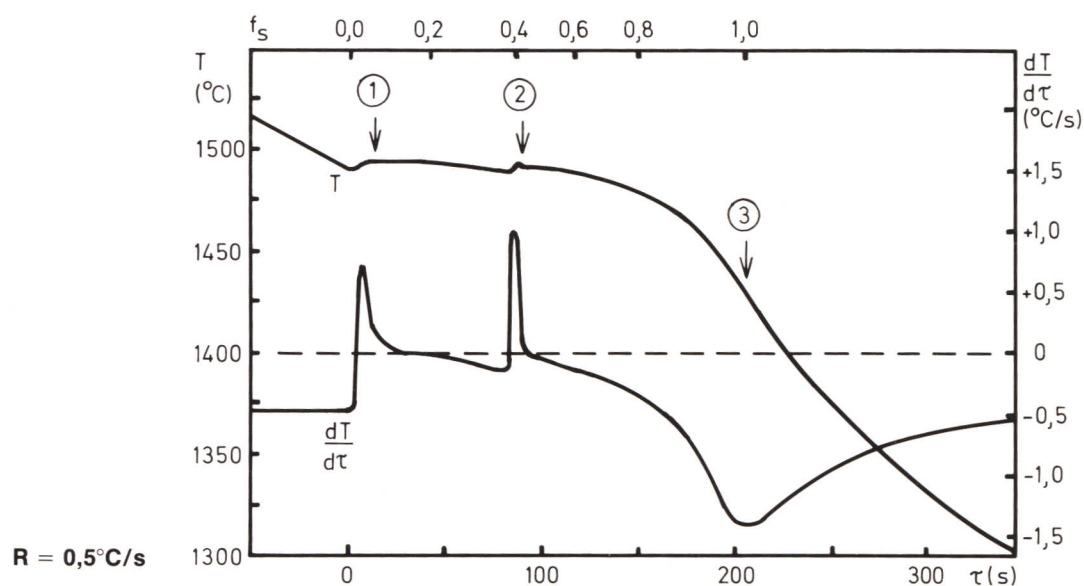
25 μm × 600

STEEL 210. 0,3% C Cr Ni Mo LOW ALLOY STEEL**Designations**

SIS	AISI	Werkstoff Nr
—	—	—

Composition (wt-%)

C	Si	Mn	P	S	Cr	Ni	Mo	Cu	V	Al _{tot}	N
0,27	0,02	0,32	0,006	0,008	1,66	3,5	0,42	0,04	0,08	0,044	0,007

Thermal Analysis

	Average Cooling Rate, R, (°C/s)		
	2,0	0,5	0,1
Liquidus temperature, ferritic primary phase, °C (1)	1487	1493	1492
Temperature of austenite formation, °C (2)	1471	1490	1490
Solidus temperature, °C (3)	1395	1430	1445
Solidification range, °C	65	60	50
Solidification time, s	80	200	640

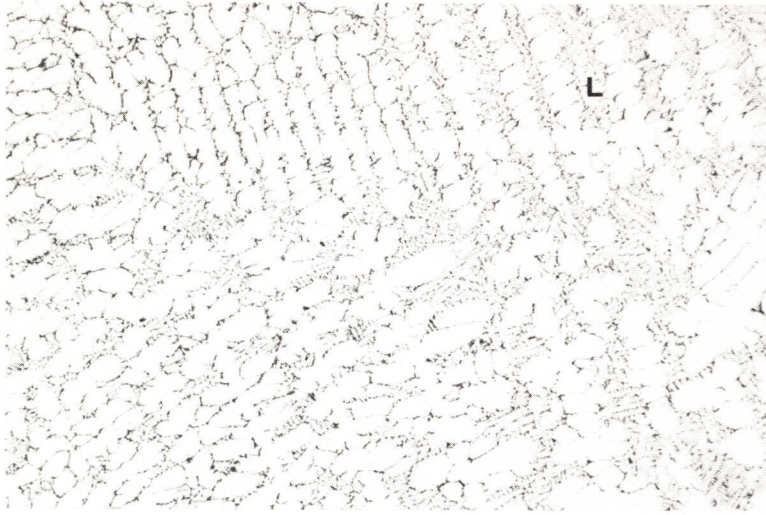
Precipitates

Very small amount of fine interdendritic carbides containing Mo and V.

Microsegregation

Element	Cr	Ni	Mo	V
I	1,6	1,3	2,2	2,0

R = 0,5 °C/s
T_q = 1350°C



Partly solidified

Figure 1

R = 0,5°C/s

T_q = 1488°C

d = 60 μm

δ-dendrites and quenched liquid (L).

400 μm × 25



Completely solidified

Figure 2

R = 2,0°C/s

T_q = 1350°C

d = 70 μm

Figures 2–4: Former δ-dendrites, transformed to γ by the peritectic reaction.

400 μm × 25

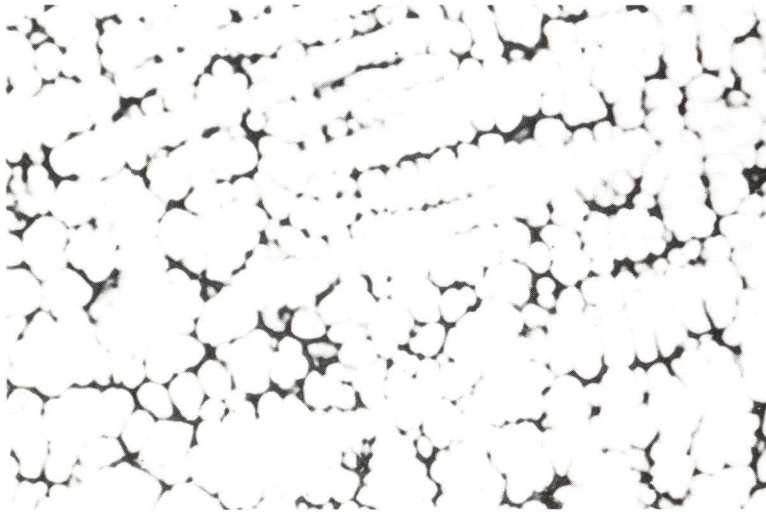


Figure 3

R = 0,5°C/s

T_q = 1350°C

d = 90 μm

400 μm × 25



Figure 4

R = 0,1°C/s

T_q = 1350°C

d = 160 μm

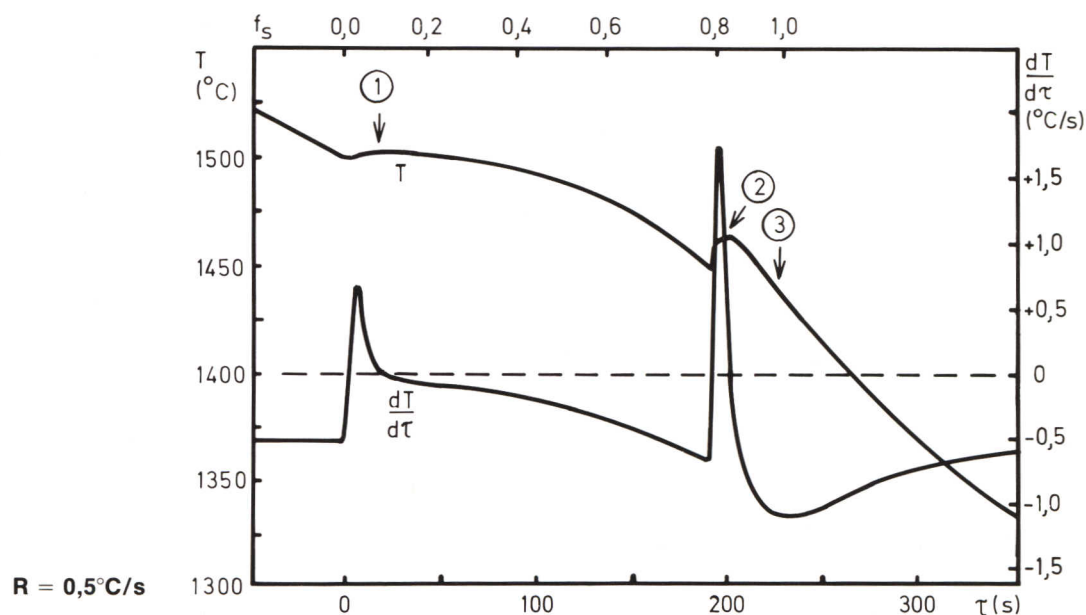
400 μm × 25

STEEL 211. 0,3% C Cr Mo LOW ALLOY STEEL**Designations**

SIS	AISI	Werkstoff Nr
2225	4130	1.7218

Composition (wt-%)

C	Si	Mn	P	S	Cr	Ni	Mo	Cu	V	Al _{tot}	N
0,29	0,21	0,62	0,012	0,006	1,11	0,15	0,21	0,04	0,04	0,011	0,004

Thermal Analysis

	Average Cooling Rate, R, ($^\circ\text{C/s}$)		
	2,0	0,5	0,1
Liquidus temperature, ferritic primary phase, $^\circ\text{C}$ (1)	1501	1501	1503
Temperature of austenite formation, $^\circ\text{C}$ (2)	1460	1471	1475
Solidus temperature, $^\circ\text{C}$ (3)	1420	1435	1450
Solidification range, $^\circ\text{C}$	85	65	55
Solidification time, s	95	220	630

Precipitates

Small amount of MnS.

Microsegregation

Element	Cr	Mo
I	1,6	2,0

$R = 0,5^\circ\text{C/s}$
 $T_q = 1360^\circ\text{C}$



Partly solidified

Figure 1

R = 0,5°C/s

T_q = 1495°C

d = 60 μm

δ-dendrites and quenched liquid (L).

400 μm × 25



Completely solidified

Figure 2

R = 2,0°C/s

T_q = 1360°C

d = 70 μm

Figures 2–4: Former δ-dendrites, transformed to γ by the peritectic reaction.

400 μm × 25

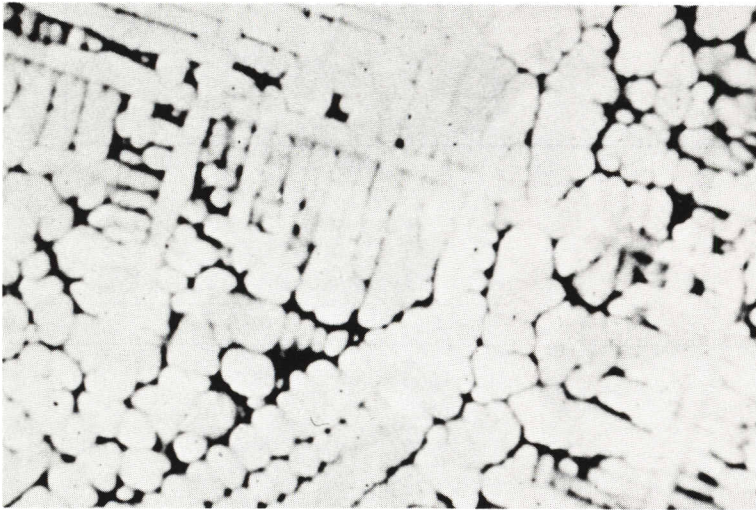


Figure 3

R = 0,5°C/s

T_q = 1360°C

d = 90 μm

400 μm × 25

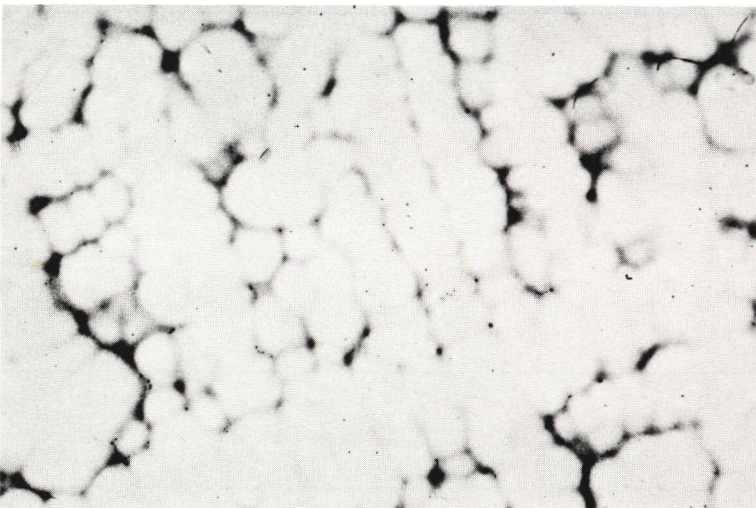


Figure 4

R = 0,1°C/s

T_q = 1360°C

d = 150 μm

400 μm × 25